

Comparison Studies of Finite Momentum Correlators on Anisotropic and Isotropic Lattices

S.Collins^{a*}, C.T.H.Davies^{a*}, J.Hein^{b*†} R.R.Horgan^{c*},
G.P.Lepage^b, J.Shigemitsu^d.

^aDepartment of Physics & Astronomy, University of Glasgow, Glasgow, G12 8QQ, UK.

^bNewman Laboratory of Nuclear Studies, Cornell University, Ithaca, NY 14853, USA.

^cD.A.M.T.P. , CMS, Wilberforce Road, Cambridge, England CB3 0WA, UK.

^dPhysics Department, The Ohio State University, Columbus, OH 43210, USA.

Abstract

We study hadronic two- and three-point correlators relevant for heavy to light pseudoscalar meson semi-leptonic decays, using Symanzik improved glue, D234 light quark and NRQCD heavy quark actions. Detailed comparisons are made between simulations on anisotropic and isotropic lattices involving finite momentum hadrons. We find evidence that having an anisotropy helps in extracting better signals at higher momenta. Initial results for the form factors $f_+(q^2)$ and $f_0(q^2)$ are presented with tree-level matching of the lattice heavy-light currents.

PACS numbers: 12.38.Gc, 13.20.He, 14.40.Nd

*UKQCD Collaboration

†Present address: Dept. of Physics & Astronomy, University of Edinburgh, Edinburgh EH9 3JZ.

I. INTRODUCTION

The use of anisotropic lattices with a finer grid in the temporal direction ($a_t < a_s$) has been advocated for studies of correlation functions that produce usable signals only over a limited time range, T_{signal} , in physical units [1]. Even when T_{signal} is reasonably large (e.g. $> 1fm$), if one is working on coarse isotropic lattices with lattice spacing $a > 0.2fm$ only a few data points will lie within T_{signal} and fitting data becomes problematic. One is then naturally led to anisotropic lattices in order to retain the advantages of working with only a small number of lattice sites in spatial directions and nevertheless have enough temporal resolution within T_{signal} . Many of the recent examples of successful employment of anisotropic lattices have been in simulations on very coarse spatial lattices. These include investigations of the glueball spectrum [2] and NRQCD studies of heavy hybrid states [3,4] and of quarkonium fine structure [5]. Anisotropic lattices have also been useful in finite temperature studies [6,7] and have been employed as an alternate approach to simulations of heavy quarks [8,9]. In several of these examples one turns to anisotropic lattices for two reasons: to be able to extract a better signal, and to avoid discretization errors coming from large $a_t M$ or $a_t E$.

In this article we investigate the extent to which anisotropic lattices could also be useful in simulations of finite momentum hadrons. We have in mind, for instance, heavy meson semi-leptonic decays such as $B \rightarrow \pi(\rho) l \nu$ [10]. In order to be able to cover the full kinematic range of interest to experimentalists and map out the q^2 dependence of form factors ($q^\mu = p^\mu - p'^\mu$ with $p^\mu =$ momentum of the decaying B meson and $p'^\mu =$ the pion momentum) one needs to calculate matrix elements between hadrons with large momenta. In the B meson rest frame, for instance, one would ideally like to simulate pions with momenta all the way from $p' \equiv |\vec{p}'| = 0$ to approximately $p' = M_B/2$. Correlators for hadrons with finite momenta are much noisier than in the zero momentum case, this being particularly true for light hadrons such as the pion. Hence one is dealing with a situation where T_{signal} is shrinking rapidly as the momentum increases. Even for reasonably fine lattices (e.g. $a_t = a_s \sim 0.1fm$) once T_{signal} falls significantly below $1fm$ one might consider going to anisotropic lattices.

To make the above statements more explicit, and come up with concrete examples that could guide us in the future, we have studied heavy meson semi-leptonic decays on both isotropic and anisotropic lattices with comparable coarse spatial lattice spacings around $a_s \approx 0.25 - 0.29fm$. Simulations of semi-leptonic decays require good control over both two- and three-point correlators. We use identical operators and smearing functions on the isotropic and anisotropic lattices. This way one creates similar signals on the initial timeslices and can watch how they propagate in time on the two lattices. We then compare the ease with which physics is extracted on the anisotropic versus the isotropic lattice. We find that at higher momenta anisotropic simulations are superior in providing more reliable signals.

Extracting a good signal is just one of the challenges one faces in lattice studies of semileptonic decays involving hadrons with high momenta. One must, for instance, also control large ap discretization errors. The second objective of the present simulations was to check how successful highly improved quark and glue actions are in removing lattice artifacts.

Working with Symanzik improved gauge actions [11], D234 light quark [12] and $O(a^2)$ improved NRQCD heavy quark [13] actions we have studied dispersion relations, speed of light renormalizations and also heavy meson decay constants at finite momenta. We find continuum-like behaviour within 5% up to about $p \sim 1.2\text{GeV}$. Even for $p \sim 1.5\text{GeV}$, which on our coarse lattices corresponds to $a_s p \sim 2$, deviations are 10% or less in many cases. Although additional tests are clearly still called for, we are very encouraged by these findings. In the future we plan to go to lattices finer than those used in the present initial study. Our experience to date indicates it may not be necessary to go very much finer to get phenomenologically meaningful results. With highly improved actions, simulations of hadrons with momenta as high as $p \sim 1.5 - 2.0\text{GeV}$ are possible once $a_s < 0.2\text{fm}$. It is not necessary to have $a_s p < 1$. We also note that the findings of the present work should carry over from the actions used here to other highly improved actions. For instance, the most highly improved light quark action with better chiral properties than the D234 action would be the staggered action [1,14]. One could also consider using heavy clover [15] rather than NRQCD heavy quarks. It will be worthwhile investigating these alternative options in the future.

In the next section we introduce the highly improved gauge and quark actions used in our study and discuss simulation parameters. In the current exploratory study, we have not tried to tune quark masses very accurately. On both the isotropic and anisotropic lattices we work with one light quark mass slightly heavier than the *strange* quark. On the anisotropic lattice we accumulated results for two heavy quark masses, one around the *bottom* quark and the other close to the *charm* quark. On the isotropic lattice only one heavy quark mass near the *bottom* quark was used. Section III concentrates on two-point function results. We compare effective masses on isotropic and anisotropic lattices and discuss dispersion relations and ratios of decay constant matrix elements for heavy mesons with and without spatial momenta. In section IV we present results for three-point functions relevant for pseudoscalar \rightarrow pseudoscalar semileptonic decays. Again comparisons are made between signals on isotropic and anisotropic lattices. The formfactors $f_+(q^2)$ and $f_0(q^2)$ are extracted.

II. GAUGE AND QUARK ACTIONS AND SIMULATION PARAMETERS

A. Gauge Actions

We use the standard Symanzik improved isotropic gauge action including square and six-link rectangular loops [11].

$$\mathcal{S}_G^{(iso)} = -\beta \sum_{x, \mu > \nu} \left\{ \frac{5}{3} \frac{P_{\mu\nu}}{u_L^4} - \frac{1}{12} \frac{R_{\mu\nu}}{u_L^6} - \frac{1}{12} \frac{R_{\nu\mu}}{u_L^6} \right\}, \quad (1)$$

with

$$P_{\mu\nu} = \frac{1}{N_c} \text{Real} \left(\text{Tr} \{ U_\mu(x) U_\nu(x + a_\mu) U_\mu^\dagger(x + a_\nu) U_\nu^\dagger(x) \} \right), \quad (2)$$

$$R_{\mu\nu} = \frac{1}{N_c} \text{Real} \left(\text{Tr} \{ U_\mu(x) U_\mu(x + a_\mu) U_\nu(x + 2a_\mu) U_\mu^\dagger(x + a_\mu + a_\nu) U_\mu^\dagger(x + a_\nu) U_\nu^\dagger(x) \} \right). \quad (3)$$

$\beta = 2N_c/g^2$ and u_L is the tadpole improvement “ u_0 ” factor, for which we use the Landau-link definition in this article [16]. For each β , u_L must be determined iteratively via simulations. One could also consider using perturbative expressions for u_L . On anisotropic lattices one can drop rectangles that extend over two links in the time direction and one has,

$$\begin{aligned} \mathcal{S}_G^{(aniso)} = & -\beta \sum_{x, s>s'} \frac{1}{\chi_0} \left\{ \frac{5}{3} \frac{P_{ss'}}{u_s^4} - \frac{1}{12} \frac{R_{ss'}}{u_s^6} - \frac{1}{12} \frac{R_{s's}}{u_s^6} \right\} \\ & -\beta \sum_{x,s} \chi_0 \left\{ \frac{4}{3} \frac{P_{st}}{u_s^2 u_t^2} - \frac{1}{12} \frac{R_{st}}{u_s^4 u_t^2} \right\}. \end{aligned} \quad (4)$$

The variables s and s' run only over spatial directions and one must now distinguish between temporal and spatial Landau-link tadpole improvement factors, u_t and u_s . χ_0 is the bare anisotropy. It differs from the true or renormalized anisotropy,

$$\chi \equiv a_s/a_t, \quad (5)$$

once quantum corrections are taken into account. Just as one fixes lattice spacings through some experimental input in conventional lattice calculations, when working on anisotropic lattices one must, in addition, determine the ratio of the spatial and temporal lattice spacings, a_s/a_t , via some physics requirement. This leads to the renormalized anisotropy χ . In the absence of lattice artifacts, it should not matter which physical quantity is used to fix χ . Conversely the dependence of χ on how it was determined provides a measure of discretization errors in the lattice system. In reference [17] the renormalized anisotropy was calculated for the action $\mathcal{S}_G^{(aniso)}$ of eq.(4) using both the torelon dispersion relation and the sideways potential method for several values of β and χ_0 . Agreement was found between the two determinations within 3-4%. We will be using those results in this article.

An alternate and equivalent procedure would be to write,

$$\begin{aligned} \mathcal{S}_G^{(aniso)} = & -\beta \sum_{x, s>s'} \frac{\eta}{\chi} \left\{ \frac{5}{3} \frac{P_{ss'}}{u_s^4} - \frac{1}{12} \frac{R_{ss'}}{u_s^6} - \frac{1}{12} \frac{R_{s's}}{u_s^6} \right\} \\ & -\beta \sum_{x,s} \frac{\chi}{\eta} \left\{ \frac{4}{3} \frac{P_{st}}{u_s^2 u_t^2} - \frac{1}{12} \frac{R_{st}}{u_s^4 u_t^2} \right\}, \end{aligned} \quad (6)$$

($\eta \equiv \chi/\chi_0$) and adjust η at fixed χ to satisfy some physical criterion.

B. Light Quark Actions

The isotropic D234 quark action is given by [12],

$$\begin{aligned} \mathcal{S}_{D234}^{(iso)} = & a^4 \sum_x \bar{\Psi}_c \left\{ \gamma_t \frac{1}{a} (\nabla_t - \frac{1}{6} C_{3t} \nabla_t^{(3)}) + \frac{C_0}{a} \vec{\gamma} \cdot (\vec{\nabla} - \frac{1}{6} C_3 \vec{\nabla}^{(3)}) + m_0 \right. \\ & \left. - \frac{ra}{2} \left[\frac{1}{a^2} (\nabla_t^{(2)} - \frac{1}{12} C_{4t} \nabla_t^{(4)}) + \frac{1}{a^2} \sum_{j=1}^3 (\nabla_j^{(2)} - \frac{1}{12} C_4 \nabla_j^{(4)}) \right] \right\} \end{aligned}$$

$$\begin{aligned}
& -ra \frac{C_F i\sigma_{\mu\nu} \tilde{F}^{\mu\nu}}{4 a^2} \left. \right\} \Psi_c \tag{7} \\
& = \sum_x \bar{\Psi} \left\{ \gamma_t (\nabla_t - \frac{1}{6} C_{3t} \nabla_t^{(3)}) + C_0 \vec{\gamma} \cdot (\vec{\nabla} - \frac{1}{6} C_3 \vec{\nabla}^{(3)}) + am_0 \right. \\
& \quad \left. - \frac{r}{2} \left[(\nabla_t^{(2)} - \frac{1}{12} C_{4t} \nabla_t^{(4)}) + \sum_{j=1}^3 (\nabla_j^{(2)} - \frac{1}{12} C_4 \nabla_j^{(4)}) \right] \right. \\
& \quad \left. - r \frac{C_F i\sigma_{\mu\nu} \tilde{F}^{\mu\nu}}{4} \right\} \Psi. \tag{8}
\end{aligned}$$

The quark fields Ψ_c and the dimensionless lattice fields Ψ are related through

$$\Psi = a^{3/2} \Psi_c. \tag{9}$$

Definitions for tadpole improved dimensionless covariant derivatives and field strength tensors are summarized for instance in the Appendix of reference [18]. We note here just the relation between unimproved $F_{\mu\nu}$ and the $O(a^2)$ improved field strength tensors $\tilde{F}_{\mu\nu}$ used in D234 actions.

$$\begin{aligned}
\tilde{F}_{\mu\nu}(x) &= \frac{5}{3} F_{\mu\nu}(x) \\
& - \frac{1}{6} \left[\frac{1}{u_\mu^2} (U_\mu(x) F_{\mu\nu}(x + a_\mu) U_\mu^\dagger(x) + U_\mu^\dagger(x - a_\mu) F_{\mu\nu}(x - a_\mu) U_\mu(x - a_\mu)) - (\mu \leftrightarrow \nu) \right] \\
& + \frac{1}{6} \left(\frac{1}{u_\mu^2} + \frac{1}{u_\nu^2} - 2 \right) F_{\mu\nu}(x). \tag{10}
\end{aligned}$$

The last term is needed so that factors of $1/u_\mu$ are correctly removed from contributions to $U F_{\mu\nu} U^\dagger$ and $U^\dagger F_{\mu\nu} U$ that end up being four link objects rather than six link ones. Effects of this term are nonnegligible on coarse lattices.

After tadpole improving the action we set the coefficients, C_{ti} , C_i , C_0 and C_F equal to their tree-level value of unity in our simulations. We also work with $r = 1$.

The anisotropic D234 action is,

$$\begin{aligned}
\mathcal{S}_{D234}^{(aniso)} &= a_s^3 a_t \sum_x \bar{\Psi}_c \left\{ \gamma_t \frac{1}{a_t} \nabla_t + \frac{C_0}{a_s} \vec{\gamma} \cdot (\vec{\nabla} - \frac{1}{6} C_3 \vec{\nabla}^{(3)}) + m_0 \right. \\
& \quad \left. - \frac{ra_s}{2} \left[\frac{1}{a_t^2} \nabla_t^{(2)} + \frac{1}{a_s^2} \sum_{j=1}^3 (\nabla_j^{(2)} - \frac{1}{12} C_4 \nabla_j^{(4)}) \right] - ra_s \frac{C_F i\sigma_{\mu\nu} \tilde{F}^{\mu\nu}}{4 a_\mu a_\nu} \right\} \Psi_c \tag{11}
\end{aligned}$$

$$\begin{aligned}
& = \sum_x \bar{\Psi} \left\{ \gamma_t \nabla_t + \frac{C_0}{\chi} \vec{\gamma} \cdot (\vec{\nabla} - \frac{1}{6} C_3 \vec{\nabla}^{(3)}) + a_t m_0 \right. \\
& \quad \left. - \frac{r}{2} \left[\chi \nabla_t^{(2)} + \frac{1}{\chi} \sum_{j=1}^3 (\nabla_j^{(2)} - \frac{1}{12} C_4 \nabla_j^{(4)}) \right] - r \frac{C_F i\sigma_{\mu\nu} \tilde{F}^{\mu\nu} a_s a_t}{4 a_\mu a_\nu} \right\} \Psi, \tag{12}
\end{aligned}$$

where we have used the spatial lattice spacing a_s to rescale the quark fields according to eq.(9). Note that the renormalised anisotropy $\chi = a_s/a_t$ appears in the quark action. In

a quenched calculation it is permissible to first fix χ in the pure glue sector and use this value for the ratio of spatial and temporal lattice spacings in the quark action. $\mathcal{S}_{D234}^{(aniso)}$ has its own ‘‘speed of light’’ renormalization term C_0 . For fixed χ this coefficient must be tuned to ensure correct dispersion relations in fermionic correlators. In the future, especially in unquenched calculations, it may be simplest to work with eq.(6) and eq.(12) at fixed χ and simultaneously and iteratively adjust η and C_0 using appropriate physics criteria. Another possibility is to use perturbative expressions for η and C_0 throughout. In the present article we will use nonperturbatively determined χ , u_L , u_s and u_t from references [12,17] and a one-loop perturbative estimate for C_0 from reference [18]. Just as in $\mathcal{S}_{D234}^{(iso)}$, we set C_3 , C_4 and C_F in $\mathcal{S}_{D234}^{(aniso)}$ equal to unity.

C. Heavy Quark Actions

It suffices to write down one expression for both the isotropic and anisotropic NRQCD actions, the former corresponding simply to $\chi = 1$ [13,19]. We work with dimensionless 2-spinor fields $\Phi = a_s^{3/2}\Phi_c$ in terms of which

$$\mathcal{S}_{NRQCD} = \sum_x \left\{ \bar{\Phi}_t \Phi_t - \bar{\Phi}_t \left(1 - \frac{a_t \delta H}{2} \right)_t \left(1 - \frac{a_t H_0}{2n} \right)_t U_4^\dagger \left(1 - \frac{a_t H_0}{2n} \right)_{t-1} \left(1 - \frac{a_t \delta H}{2} \right)_{t-1} \Phi_{t-1} \right\}. \quad (13)$$

H_0 is the nonrelativistic kinetic energy operator,

$$a_t H_0 = -\frac{\Delta^{(2)}}{2\chi(a_s M_0)}, \quad (14)$$

and δH includes relativistic and finite-lattice-spacing corrections,

$$\begin{aligned} a_t \delta H = & -c_1 \frac{1}{2\chi(a_s M_0)} \boldsymbol{\sigma} \cdot \tilde{\mathbf{B}} \\ & + c_2 \frac{i}{8(a_s M_0)^2} (\nabla \cdot \tilde{\mathbf{E}} - \tilde{\mathbf{E}} \cdot \nabla) - c_3 \frac{1}{8(a_s M_0)^2} \boldsymbol{\sigma} \cdot (\tilde{\nabla} \times \tilde{\mathbf{E}} - \tilde{\mathbf{E}} \times \tilde{\nabla}) \\ & - c_4 \frac{(\Delta^{(2)})^2}{8\chi(a_s M_0)^3} + c_5 \frac{\Delta^{(4)}}{24\chi(a_s M_0)} - c_6 \frac{(\Delta^{(2)})^2}{16n\chi^2(a_s M_0)^2}. \end{aligned} \quad (15)$$

All derivatives are tadpole improved and,

$$\Delta^{(2)} = \sum_{j=1}^3 \nabla_j^{(2)}, \quad \Delta^{(4)} = \sum_{j=1}^3 \nabla_j^{(4)} \quad (16)$$

$$\tilde{\nabla}_k = \nabla_k - \frac{1}{6} \nabla_k^{(3)} \quad (17)$$

The dimensionless Euclidean electric and magnetic fields are,

$$\tilde{E}_k = \tilde{F}_{k4}, \quad \tilde{B}_k = -\frac{1}{2} \epsilon_{ijk} \tilde{F}_{ij} \quad (18)$$

∇_k , $\nabla_k^{(j)}$, $j = 2, 3, 4$ and $\tilde{F}_{\mu\nu}$ are the same as in the light quark actions of the previous subsection. In our simulations we again set all $c_i = 1$.

D. Simulation Parameters

Simulations have been carried out on $8^3 \times 20$ isotropic and $8^3 \times 48$ ($\chi = 5.3$) anisotropic lattices using ensembles of 200 configurations each. Details are summarized in Table I. The β , u_0 and a^{-1} values are taken from reference [12] for the isotropic and from reference [17] for the anisotropic lattices, respectively. The latter reference also provided χ_0 and χ . None of the lattice spacing determinations are very precise. For the anisotropic lattice we have taken the 4.503GeV quoted in [17] for a_t^{-1} from Υ S-P splittings and reduced it by 22%, approximately the amount by which light hadron a^{-1} values differ from those fixed by Υ splittings in quenched calculations. This is also consistent with [17]’s finding for a^{-1} from the string tension. In heavy-light physics one expects light hadron a^{-1} values to be more appropriate. The “speed of light” renormalization coefficient C_0 was estimated from the one-loop perturbative result for $\chi = 5.3$, $C_0 = 1 - 0.45\alpha_s$ [18], using $\alpha_s \approx 0.4$.

The bare light quark mass has been adjusted so that one has the same pseudoscalar-to-vector ratio, P/V, on the isotropic and anisotropic lattices. We found that this required approximately a factor of 3/2 more BiCGstab iterations to create light quark propagators on the anisotropic lattice compared to on the isotropic one (actual numbers are given in Table I). We believe the reason is critical slowing down due to an increase in the condition number with a_t^{-1} . Although our pion is still quite heavy ($\sim 840\text{MeV}$), on the anisotropic lattice we did, on a few occasions, encounter problems with “exceptional” configurations. In the process of accumulating an ensemble of 200 configurations, 5 had to be skipped. We will see below that the anisotropic pion propagators are noisier than the isotropic ones for the same pion mass. Other mesons such as the ρ and B , which use the same light quark propagators are not affected, however. Although this aspect of simulations on anisotropic lattices is worrisome and needs further study, we do not, at the moment, believe that this implies anisotropic lattices will never be useful for light quarks. The problem has been exaggerated in the present calculations since we are on very coarse spatial lattices and $\chi = 5.3$ is a large anisotropy. In future, more realistic, simulations we plan to use finer lattices and work with moderate anisotropies such as $\chi = 2 - 3$. We expect to be able to go to lighter pions there without encountering problems. We mention that the tadpole improvement adopted in eq.(10) leads to a larger effective “ c_{SW} ” than has been used in the past, and it is known that large c_{SW} , such as the nonperturbative c_{SW} , leads to problems on coarse lattices. This phenomenon appears to set in at heavier quark masses when $\chi > 1$. There were no hints of problems with exceptional configurations on our coarse isotropic lattice for the light quark masses considered.

III. RESULTS FROM TWO POINT FUNCTIONS

We calculated two-point correlators for the light-light pseudoscalar and vector, the B_s and B_s^* and, on the anisotropic lattice, also for the D_s and D_s^* mesons. We will generically call these the “pion”, “rho”, “B meson” and “D meson” channels respectively. Current sinks corresponding to the temporal and spatial components of the heavy-light axial vector currents were also considered. We employed gauge invariant smearings, separately for the light and heavy quarks, of the form

$$(1 + c_{sm}\Delta^{(2)})^l \delta^{(3)}(\vec{x} - \vec{x}_0). \quad (19)$$

For light quarks we used $l = 10$ and $c_{sm} = 1/12$. We have two smearings for the heavy quarks both with $c_{sm} = 1/24$ but with different l values, $l_1 = 2$ and $l_2 = 10$. We found that l_2 works better for zero and low momentum B mesons and l_1 gives better signals for higher momentum correlators. We accumulated data at 7 spatial momenta, $(0,0,0)$, $(0,0,1)$, $(0,1,1)$, $(1,1,1)$, $(0,0,2)$, $(0,2,2)$ and $(0,0,3)$ in units of $2\pi/aL$, averaging over all equivalent momenta. In the following subsections we will compare effective masses, present fit results for a small number of states and dispersion relations, and look at ratios of matrix elements with current sinks.

A. Effective Masses

We start by comparing raw data for B meson correlators on the anisotropic and isotropic lattices. Figs. 1. and 2. show fractional errors of the correlators versus physical time for several momenta. One sees that, where there is overlap, the fluctuations of B correlators are identical on the two lattices. Effective mass plots are presented in Figs. 3 to 5 for the B meson for three representative momenta. Each figure shows results in lattice units on the left and results in physical units, using central values of the scales from Table I, on the right. We label time slices such that sources are at $t = 0$. By looking at the anisotropic data one finds plateaus starting at about $t = 0.3\text{fm} - 0.4\text{fm}$ for all momenta. This must also be the case for the isotropic data since the original signals are essentially the same. However, based only on information from the isotropic data, this is not always obvious, especially for the higher momenta. There is also an unfortunate upward fluctuation at around $t = 0.7\text{fm}$ which makes fitting the isotropic data more difficult. One agonizes over whether to fit starting before or after the hump. This illustrates some of the immediate advantages of anisotropic lattices. Once a plateau has set in it is more easily recognized, and one is also less sensitive to one or two points fluctuating up or down, since there are enough other points around.

Effective mass plots for pions and rhos are given in Figs. 6 - 9 and corresponding correlator fractional errors in Figs. 10 and 11. In contrast to the B meson case, one sees that fluctuations are considerably larger for the pion correlators on anisotropic lattices. This indicates that some configurations are close to being “exceptional”. The rho correlators show no enhanced errors relative to the isotropic lattice. Despite the larger fluctuations, it is not difficult to fit the anisotropic pion data and fluctuations cancel to some degree upon calculating physical quantities such as dispersion relations or semi-leptonic formfactors. In Fig. 12 we show fitted energies for the anisotropic lattice pion and rho at momentum $(1,1,1)$ versus t_{min}/a_t from single cosh fits. The pion energies have larger errors but look otherwise normal. In future simulations one will have to monitor pion correlators carefully.

Meson correlators were calculated up to the center of the lattice in the time direction. We find that for zero and low momenta T_{signal} covers the entire $T/2$ region (1.24fm for the anisotropic and 2.25fm for the isotropic lattice). However as the momentum increases T_{signal} starts to shrink. For the B meson this occurs only at the highest two momenta $(0,2,2)$ and $(0,0,3)$. For the pion and the rho, T_{signal} shrinks below $\sim 1\text{fm}$ once one goes

beyond momentum (1,1,1). It then becomes much harder to get reliable information from the isotropic lattice. For instance, it should be obvious from Fig. 9 that trying to fit the isotropic data is considerably more frustrating than carrying out fits to the anisotropic data. Fig. 13 shows fitted energies versus t_{min}/a_t for the isotropic rho and pion with momentum (1,1,1). This should be compared with the corresponding anisotropic results in Fig. 12. With the isotropic data, picking t_{min} is extremely tricky. In past work on isotropic lattices we often adopted a criterion whereby if $t_{min}^{(0)}$ is the smallest t_{min} which gives an acceptable Q -value (> 0.1) then our preferred choice for t_{min} in a single exponential (cosh) fit to a single correlator would be $t_{min}^{(0)} + 2a_t$ [20,21]. This is a fairly conservative criterion leading to larger statistical errors than if one chooses a smaller t_{min} . We will call fits using this criterion “B-fits”. In the present calculation, B-fits would dictate $t_{min}/a_t = 3$ or 4 for most of our fits to isotropic data. We will abide by this t_{min} for fitting B meson correlators. However, for the rho and the pion we will be less conservative and use $t_{min}/a_t = 2$, which is equal to 0.5fm in physical units. Q -values are always acceptable already for $t_{min}/a_t = 2$. We call this latter choice “A-fits”. Based only on the isotropic data, one would be hard pressed to argue why A-fits should be preferred over B-fits. In the present comparison study, however, we have additional information from the anisotropic lattice that tells us that plateaus have set in by $t \sim 0.3 - 0.4$ fm, i.e. before $t = 0.5$ fm, and hence A-fits should be fine. We should also note that correlated fits were used throughout our analysis.

The results presented in this subsection demonstrate that for the pion and rho correlators there is a clear advantage to anisotropic simulations starting with momenta around (1,1,1). For B correlators benefits start around (0,2,2). Below we will present physics results extracted from the isotropic and anisotropic lattices, concentrating on momentum dependent quantities. For the B meson on both lattices and the pion and rho on the anisotropic lattice we can go to the highest momentum (0,0,3). On the isotropic lattice, pion and rho results can only be extracted up to momentum (0,0,2) using A-fits. With B-fits, only momenta up to (1,1,1) can be reached and errors are larger than with A-fits.

Another lesson to be drawn from the present exercise is the importance of good smearings. We can get away here with single exponential (cosh) fits, because our smearings are reasonable and plateaus set in well within T_{signal} . In the case of poorer smearings it would still be advantageous to be on an anisotropic lattice with many data points within T_{signal} , since that would facilitate multi-exponential fits. Going to lattices with longer time extent in physical units in search of a plateau will not work for high momentum correlators since T_{signal} stops well before the end of the lattice. It is much more profitable to explore better smearings and/or increase the number of points within T_{signal} .

B. Dispersion Relation

A convenient way to investigate how well lattice simulations are reproducing relativistic dispersion relations is to consider the following quantity [12],

$$C(p) \equiv \sqrt{\frac{E^2(p) - E^2(0)}{p^2}}, \quad (20)$$

where $p \equiv |\vec{p}|$ and $E(p)$ is the total energy of the particle. In a relativistic theory $C(p) = 1$ for all p . $C(p)$ is shown for the pion and the rho in Figs. 14 and 15. One sees that on both the isotropic and anisotropic lattices, continuum behavior is observed to better than $\sim 5\%$ for momenta of up to 1.2GeV at the minimum and, in the case of the rho, even beyond that. Hence, it appears one can simulate particles with momentum as high as $p \approx 1.5/a_s$ to $2.0/a_s$ without introducing large discretization errors. One notices slightly better behavior on isotropic compared to on anisotropic lattices for the smaller momentum points. The anisotropic results are more sensitive to the tuning of C_0 , for which we have used the one-loop estimate. We have studied the effect of this one-loop correction by calculating anisotropic light quark propagators with $C_0 = 1$ on a subset of 50 configurations (at the same time adjusting $a_t m_0$ to get the same pion mass). The fancy squares in Fig.16 show results for $C(p)$ for $C_0 = 1$, i.e. without the one-loop correction. They are compared with results from 50 configurations using $C_0 = 0.82$. For completeness we also include corresponding points from Figs.14 and 15, which are based on the full set of 200 configurations with $C_0 = 0.82$. Although effects from the one-loop correction are not large, nevertheless, they are crucial for getting the $\sim 2\%$ to $\sim 5\%$ agreement with relativistic behavior. Even if we had attempted to tune C_0 nonperturbatively, it would have been difficult to do much better simultaneously for both pions and rhos, than our perturbative estimate. The errors on $C(p)$ for anisotropic pions (from a bootstrap analysis) are smaller than one might have expected based on the large fluctuations noted above in pion correlators. We are evidently observing large cancellations between fluctuations in the zero and nonzero momentum correlators.

The isotropic results in Figs. 14 and 15 are based on A-fits, defined above. In Fig. 17 we compare with results using B-fits. Results from the two different fits are consistent. But, as expected, errors are much larger for B-fits and one cannot go beyond the three lowest momenta using them. Unless specified otherwise, for the rest of this article we will use A-fits for pions and rhos on isotropic lattices. The isotropic results in Figs. 14 and 15 are also consistent with findings in reference [12], where comparisons were made with clover quarks at similar lattice spacings. In those studies $C(p)$, at lattice spacing $a = 0.25fm$, was consistent with unity within errors up to about $p = 1.2GeV$ for the D234 quark action and exhibited $10\% \sim 20\%$ deviations from unity for the clover quark action.

$C(p)$ is not applicable for heavy-light mesons involving NRQCD heavy quarks. The NRQCD action omits the heavy quark rest mass and meson correlators fall off with an energy $E_{sim}(p)$ that differs from the total energy $E(p)$. However one has,

$$\delta E(p) \equiv E_{sim}(p) - E_{sim}(0) = E(p) - E(0), \quad (21)$$

and one can define the “kinetic” mass, $M_{kin} = M_2$ through,

$$M_{kin} = (p^2 - \delta E^2(p))/(2 \delta E(p)). \quad (22)$$

If $E_{sim}(p)$ has the correct momentum dependence, then M_{kin} should be independent of the momentum used in the RHS of eq.(22). Fig.18 shows M_{kin} for several mesons versus the momentum of the correlator from which it was extracted. On the anisotropic lattice we have data for two heavy-light mesons, both the B_s and the D_s . The latter meson uses NRQCD charm quarks. One sees that for all mesons, results for M_{kin} are independent of momentum

within errors up to about $p \sim 1.5\text{GeV}$. For the pion and the rho we can also compare M_{kin} with the rest mass $M_1 \equiv E(0)$. The deviation of M_{kin} from M_1 reflects the deviation of $C(p)$ from unity in Figs.14 and 15 and, like the latter, is very small.

C. Decay Constant Ratios

Heavy meson semi-leptonic decay formfactors, which will be the focus of the next section, require matrix elements of heavy-light currents between hadronic states with and without momentum. It is worthwhile considering first simpler matrix elements of currents between mesons and the vacuum and studying their momentum dependence. Such matrix elements are relevant for meson leptonic decays. Starting from the usual definition of the decay constant (in Euclidean space),

$$\langle 0 | A_\mu | B, \vec{p} \rangle = \tilde{p}_\mu f_B, \quad (23)$$

($\tilde{p}_\mu = (iE, \vec{p})$) one can form the ratio,

$$\frac{\langle 0 | A_0 | PS, \vec{p} \rangle / \sqrt{E(p)}}{\langle 0 | A_0 | PS, \vec{p} = 0 \rangle / \sqrt{M_{PS}}} = \frac{\sqrt{E(p)}}{\sqrt{M_{PS}}}. \quad (24)$$

This ratio was studied recently on finer lattices using a less improved action [22] (similar calculations were done several years ago with relativistic heavy fermions in [23]). In the present article we will use the following current for the temporal component of the axial vector current,

$$A_0 \rightarrow J_{A_0}^{(0)} = \bar{\Psi} \gamma_5 \gamma_0 Q, \quad (25)$$

where Ψ is the light quark field and the heavy quark 4-spinor Q has the NRQCD 2-spinor Φ as the upper two components and zero for the lower two components. The superscript (0) signifies that $J_{A_0}^{(0)}$ is the zeroth order term in an $1/M$ expansion for the axial vector current. The LHS of eq.(24) is replaced by,

$$R^{(0)}(p) \equiv \frac{\langle 0 | J_{A_0}^{(0)} | \vec{p} \rangle / \sqrt{E(p)}}{\langle 0 | J_{A_0}^{(0)} | \vec{p} = 0 \rangle / \sqrt{M_{PS}}}. \quad (26)$$

In reference [22] $1/M$ current and one-loop matching corrections were included in the ratio and seen to have only a small effect relative to using just the zeroth order current for heavy quark masses around the b -quark mass. Matching calculations for the actions of the present article have not been carried out yet so we are forced to use the simple ratio $R^{(0)}(p)$ here. Figs. 19 and 20 show $R^{(0)}$ for the B_s and D_s leptonic decays, compared with the expected continuum behavior of the RHS of eq.(24). One sees good agreement for most of the momentum range studied. Only at the highest momentum ($> 1.5\text{GeV}$) does one see $\sim 15\%$ deviations for B_s mesons. One should be able to reduce these errors below $\sim 10\%$ by going to slightly finer lattices. Since we do not include higher order (in p/M) current corrections one expects agreement with full continuum QCD behavior to be worse for the D_s meson, especially at higher momenta [24]. The better agreement found in Fig. 20 as compared to in Fig. 19 is, hence, fortuitous.

D. Zero Momentum Spectrum

In the process of studying momentum dependence of meson correlators we have also accumulated some zero momentum spectrum results. They are summarized in Table II. The first errors are statistical and the second represent errors coming from uncertainties in a^{-1} which we take to be roughly 10% not including quenching effects. In this exploratory study we will not try to estimate other systematic errors. One sees that the “pion” and the “rho” masses are very close to each other on the isotropic and anisotropic lattices. The isotropic B_s meson is about 250 MeV too heavy and the anisotropic one about 600 MeV too light compared to experiment. On the other hand, the uncertainty coming from a^{-1} is at the 500-600 MeV level.

It is amusing that the heavy-light hyperfine splittings, which have been the bane of lattice heavy-light spectroscopy in the past, agree so well here with experiment for both the B_s and D_s mesons. One should not make too much out of this, however, until results at other lattice spacings have been obtained. At the moment we have no estimate of the size of scaling or unquenching corrections to this quantity. If one corrects approximately for the incorrect heavy quark mass in our simulations and multiplies by a factor of [calculated meson mass]/[experimental meson mass], then the entries in Table II for the $B_s^* - B_s$ hyperfine splitting, are modified to 48MeV or 40MeV for isotropic and anisotropic lattices respectively. Similarly the $D_s^* - D_s$ splitting becomes 148MeV. All these numbers are much larger than and in better agreement with experiment than in previous lattice estimates [21,25–29]. One difference between the present and previous calculations lies in the last term in eq.(10) which enhances $\tilde{F}_{\mu\nu}$. It is hard to imagine, however, that this term alone can be the whole story. It will be interesting to see what happens after systematic errors have been investigated more thoroughly and various corrections to the present calculation have been incorporated.

IV. RESULTS FROM THREE POINT FUNCTIONS

For pseudoscalar to pseudoscalar semi-leptonic decays one is interested in matrix elements of the heavy-light vector current V^μ . The matrix elements are then parametrized in terms of form factors f_+ and f_- (or f_1 and f_0).

$$\langle \pi(p') | V^\mu | B(p) \rangle = f_+(q^2)(p^\mu + p'^\mu) + f_-(q^2)(p^\mu - p'^\mu), \quad (27)$$

where $q^2 = (p^\mu - p'^\mu)^2$. We will write formulae for B decays but they apply also to D decays. f_1 and f_0 are defined as :

$$f_0 = f_+ + \frac{q^2}{(M_B^2 - M_\pi^2)} f_- \quad , \quad f_1 = f_+ \quad (28)$$

Our main goal in this section will be to compare the quality of signals for matrix elements such as those in eq.(27) between isotropic and anisotropic lattices. Since the light quarks in this study are still heavier than the strange quark, the physical situation we are simulating will be closest to B_s or D_s decays into Kaons.

A. Current Matrix Elements

In order to extract the matrix element of eq.(27) one starts from the following three-point function, $G_\mu^{(3)}(\vec{p}, \vec{p}', t_B, t)$, on the lattice (for technical reasons it is more convenient to consider the time reversed matrix element)

$$G_\mu^{(3)}(\vec{p}, \vec{p}', t_B, t) = \sum_{\vec{x}} \sum_{\vec{y}} e^{-i\vec{p}\cdot\vec{x}} e^{i(\vec{p}-\vec{p}')\cdot\vec{y}} \langle 0 | \Phi_B(t_B, \vec{x}) V_\mu^L(t, \vec{y}) \Phi_\pi^\dagger(0) | 0 \rangle. \quad (29)$$

Φ_π^\dagger and Φ_B^\dagger are interpolating operators used to create the pion or B meson respectively. V_μ^L is the dimensionless Euclidean space lattice heavy-light vector current. It will be defined more precisely below. It is related to the continuum Minkowski space V^μ through,

$$V_\mu^L = a_s^3 \sqrt{Z_q^{(0)}} \xi(\mu) V^\mu. \quad (30)$$

$Z_q^{(0)}$ is the tree-level wave function renormalization for lattice light quark actions. It is discussed for the isotropic and anisotropic D234 actions in the Appendix. $\xi(\mu)$ is the conversion factor between Euclidean and Minkowski space quark bilinear currents which is necessary due to the different γ -matrix conventions in the two spaces. $\xi(0) = 1$ and $\xi(k) = -i$, $k = 1, 2, 3$. t_B denotes the time slice at which the B meson operator is inserted. In the simulations t_B is kept fixed and we vary t , the timeslice of the current insertion, between 0 and t_B . Physics is extracted from those timeslices where the corresponding two-point correlators are dominated by the ground state and where $e^{-E_\pi(T-t)}$ can be ignored relative to $e^{-E_\pi t}$, T being the time extent of the lattice. If these conditions are satisfied the three-point correlator (29) becomes,

$$G_\mu^{(3)}(\vec{p}, \vec{p}', t_B, t) \rightarrow \frac{\langle 0 | \Phi_B | B(\vec{p}) \rangle \langle B(\vec{p}) | V_\mu^L | \pi(\vec{p}') \rangle \langle \pi(\vec{p}') | \Phi_\pi^\dagger | 0 \rangle}{(2E_B a_s^3) (2E_\pi a_s^3)} e^{-E_B^{sim}(t_B-t)} e^{-E_\pi t}. \quad (31)$$

The exponential factors in eq.(31) can be removed by dividing with the appropriate two-point functions.

$$\begin{aligned} G_B^{(2)}(\vec{p}, t) &= \sum_{\vec{x}} e^{-i\vec{p}\cdot\vec{x}} \langle 0 | \Phi_B(t, \vec{x}) \Phi_B^\dagger(0) | 0 \rangle \\ &\rightarrow \frac{|\langle B(\vec{p}) | \Phi_B^\dagger | 0 \rangle|^2}{(2E_B a_s^3)} e^{-E_B^{sim} t} \equiv \zeta_{BB} e^{-E_B^{sim} t}, \end{aligned} \quad (32)$$

$$G_\pi^{(2)}(\vec{p}', t) \rightarrow \frac{|\langle \pi(\vec{p}') | \Phi_\pi^\dagger | 0 \rangle|^2}{(2E_\pi a_s^3)} [e^{-E_\pi t} + e^{-E_\pi(T-t)}] \approx \zeta_{\pi\pi} e^{-E_\pi t}. \quad (33)$$

The matrix element of the continuum current V^μ can now be obtained from,

$$\Gamma_\mu^{(3)}(\vec{p}, \vec{p}', t_B, t) \equiv \xi^*(\mu) \frac{G_\mu^{(3)}(\vec{p}, \vec{p}', t_B, t)}{G_B^{(2)}(\vec{p}, t_B - t) G_\pi^{(2)}(\vec{p}', t)} \sqrt{\zeta_{BB} \zeta_{\pi\pi}} \quad (34)$$

$$\rightarrow \sqrt{Z_q^{(0)}} \frac{\langle B(\vec{p}) | V^\mu | \pi(\vec{p}') \rangle}{2\sqrt{E_B E_\pi}} \equiv \langle \tilde{V}^\mu \rangle. \quad (35)$$

Eqs. (34) and (35) relate the three- and two-point functions evaluated in our simulations to the continuum matrix elements of eq.(27). We need to specify now the lattice current V_μ^L that enters into the three-point functions. It is defined in terms of Euclidean space γ -matrices $\gamma_\mu = \xi(\mu) \gamma_{(Mink.)}^\mu$. Since we use the NRQCD formulation of heavy quarks, V_μ^L becomes an expansion in $1/M$, the inverse of the heavy quark mass. After matching to continuum QCD one has,

$$V_\mu^L = \sum_j C_j^{(V_\mu)} J_{V_\mu}^{(j)}. \quad (36)$$

For $j = 0$ one has the zeroth order, $\mathcal{O}((1/M)^0)$, current,

$$J_{V_\mu}^{(0)} = \bar{\Psi} \gamma_\mu Q, \quad (37)$$

with the fields Ψ and Q defined as in eq.(25). Higher order currents ($j > 0$) are listed in reference [30]. The matching coefficients $C_j^{(V_\mu)}$ are not yet known beyond tree-level so we will work with $C_0^{(V_\mu)} = 1$ and all other C_j 's equal to zero. One of the $1/M$ current corrections $J_{V_\mu}^{(1)}$ has $C_1^{(V_\mu)} = 1 + \mathcal{O}(\alpha_s)$ and also contributes at tree-level. However, its matrix elements include power law terms that will not be cancelled unless a proper one-loop calculation has been carried out. Hence, we do not include $J_{V_\mu}^{(1)}$ contributions in the present study.

We have evaluated $\Gamma_\mu^{(3)}(\vec{p}, \vec{p}', t_B, t)$ of eq.(34) for several pion momenta \vec{p}' ranging from (0,0,0) to (0,0,3) in units of $2\pi/(aL)$. The B meson momentum was always set equal to zero. On the anisotropic lattice we used $t_B/a_t = 24$ and on the isotropic lattice $t_B/a_t = 10$. Figs. 21 and 22 show $\Gamma_0^{(3)}$ versus t in physical units for zero momentum and for three nonzero momenta. One sees that, where there is overlap, anisotropic and isotropic lattices give consistent results. One is interested, of course, in the region where $\Gamma_0^{(3)}$ is independent of t implying that the simple t -dependence in eq.(31) and the last expression in eq.(33) is justified. $\Gamma_0^{(3)}$ can then be identified with the asymptotic matrix element $\langle \tilde{V}^0 \rangle$ of eq.(35). Again the crucial question for the higher momentum isotropic results becomes whether one would believe in the presence of a plateau if one did not have the comparison anisotropic data. To illustrate this point we show $\Gamma_0^{(3)}$ versus t in lattice units separately for isotropic and anisotropic lattices in Figs. 23 to 26. One might still feel comfortable extracting a signal from the (1,1,1) isotropic data. One would be hard pressed, however, to claim that a plateau has been established at momentum (0,0,2) based solely on the left hand plot in Fig.26. Note that T_{signal} , the time range over which statistical errors are under control, is about $1fm$ for momentum (1,1,1) and has shrunk to about $0.5fm$ for (0,0,2). We saw in the previous section that individual two-point correlators had reached a plateau by $0.3 \sim 0.4fm$. If sufficient data points could be introduced between $0.3fm$ and $0.5fm$, then one should be able to extract meaningful results for $\langle \tilde{V}^0 \rangle$. Hence, once again one sees an advantage to using anisotropic lattices starting with momentum (1,1,1). This is the same situation as with the pion and rho correlators described in the previous section, not a surprising finding since statistical errors in $\Gamma_\mu^{(3)}$ are dominated by the pion correlator and not by the B correlator.

From the region where $\Gamma_\mu^{(3)}$ is independent of t , one can extract $\langle \tilde{V}^\mu \rangle$. We show $\langle \tilde{V}^0 \rangle$ and $\langle \tilde{V}^k \rangle$ in Fig. 27 as a function of the pion momentum p' . For points at the largest momenta on

the anisotropic lattice one could be seeing some discretization effects. Only a more careful analysis involving simulations at several lattice spacings and/or further studies with nonzero B meson momenta will be able to shed more light on this. Here we are concentrating mainly on whether signals can be extracted, postponing scaling studies for the future. This is in contrast to the two-point correlator studies of the previous section where several continuum expectations based just on simple Lorentz symmetry considerations could be tested.

B. Form Factors $f_+(q^2)$ and $f_0(q^2)$

From (35), (27) and (28) one can extract the form factors $f_+(q^2)$ and $f_0(q^2)$. Isotropic lattice results for the B_s meson are shown in Fig. 28 and anisotropic lattice results for the B_s and D_s mesons in Figs. 29 and 30. The kinematics, including the range in q^2 that is covered, depends on the meson masses of Table II and differs for the two types of lattices. The errors in the three figures are statistical and come from a simultaneous bootstrap analysis of the V^0 and V^k three-point functions and the B (or D) and pion correlators.

Since we have at present only tree-level matching of the heavy-light currents and also have not tuned (or extrapolated in) the heavy and light quark masses, the above form factor results cannot be applied yet to phenomenology. What is important, however, is that with just 200 configurations it was possible to obtain form factors for a nontrivial range in q^2 and that we were able to demonstrate the advantages of anisotropic lattices in calculations of this kind. By increasing statistics in the future one should be able to get good data over an even wider range in q^2 . At that point one would also want to go to finer lattices and work with improved currents so that finite momentum errors are minimized even at the largest momenta for which signals can be obtained.

V. SUMMARY

This article investigates the extent to which anisotropic lattices can help in extracting better signals from two- and three-point correlators involving high momentum hadrons and whether they can play an important role in studies of semi-leptonic heavy meson decays into light hadrons. To address this question we have carried out simulations of heavy meson semi-leptonic decays, in parallel, on isotropic and anisotropic lattices. In order to have a meaningful comparison, we work with similar coarse spatial lattice spacings and use identical sources and smearings on the two lattices.

We find that it is considerably easier to extract reliable signals from anisotropic simulations once the light hadron momentum reaches $(1,1,1) 2\pi/(a_s L)$ or higher. This advantage may not be so obvious just by comparing Figs. 28 and 29 and one needs to go back to figures such as Fig. 22 to fully appreciate how much the anisotropy is helping here. The last point (at the smallest value of q^2) in Fig. 28 comes from the isotropic data in the left hand plot of Fig. 22 (see also Fig. 25). It is because the first three isotropic points in Fig. 22 agree with the anisotropic data, that one feels confident about the form factor results in Fig. 28. Without the anisotropic data, one would have to allow for a considerable additional systematic error, which one might call “fitting error” or “ t_{min} dependence error”,

when presenting isotropic results. Hence, the main conclusion from the present work is that anisotropic lattices definitely improve signal quality and should be considered in semi-leptonic decay studies, especially if a large range in q^2 is of interest.

The advantages of anisotropic lattices come at a certain price. For instance, such lattices require more sites in the time direction. Also light quark inversions take more iterations in order to get the same pion-to-rho mass ratio P/V . In the present simulations, the cost increase from just these two effects meant a factor of $2.4 \times 1.5 = 3.6$ in CPU time. Working with anisotropic lattices also requires tuning of more parameters. At a minimum, two additional parameters, η in the glue action and C_0 in the D234 quark action must be determined nonperturbatively or perturbatively. It is important that efficient procedures for carrying out such tunings be developed. Another drawback in the current anisotropic simulations was the increased susceptibility to exceptional configurations. If it were not for this problem and the larger fluctuations in pion correlators, the anisotropic results for the form factors $f_0(q^2)$ and $f_+(q^2)$ would have been of even higher quality relative to those coming from isotropic lattices. There are several ways one could try and ameliorate this problem in the future. Just going to finer lattices and working with more moderate anisotropies, $\chi < 5.3$, should help. One could also explore other light quark actions that have better chiral properties than the clover or D234 actions, such as highly improved staggered fermions [1,14], domain wall fermions [31] or the twisted QCD approach [32].

Ultimately one will have to weigh the additional costs associated with anisotropic lattices against the likelihood that an isotropic simulation with much higher statistics will allow us to approach the high momenta we are seeking. Based on our (and also other peoples') experience to date, we do not believe isotropic lattices can be competitive at high momenta. Signal-to-noise of high momentum correlators will be decreasing exponentially with t . When a_t is large it will be very costly to move even one additional point from the noise into T_{signal} . In order to do so one will need to reduce errors by roughly a factor of $e^{a_t(E(p)-E0)}$, where $E0$ is the ground state energy [33]. In other words, one will need an increase in statistics by a factor of $N_{stat} \equiv |e^{a_t(E(p)-E0)}|^2$. Typical numbers for the current isotropic simulation for momenta starting with (1,1,1) and higher, would be $N_{stat} \approx 4 - 10$. This means a factor of 16 - 100 if one wants to go from just one or two points in T_{signal} to a marginally useful T_{signal} of 3 to 4 points. This is much more than the cost of going to anisotropic lattices.

We mention another unrelated advantage of anisotropic actions. One difference between $\mathcal{S}_G^{(iso)}$ and $\mathcal{S}_G^{(aniso)}$ is the omission in the latter of rectangles that span two links in the time direction. Similarly $\mathcal{S}_{D234}^{(iso)}$ includes higher time derivatives that are absent in $\mathcal{S}_{D234}^{(aniso)}$. As a consequence, for the same amount of improvement in spatial directions, the anisotropic actions suffer less from lack of reflection positivity and/or presence of ghosts. In addition to being theoretically cleaner this means perturbation theory is more straightforward for the anisotropic actions. One such example is the $Z_q^{(0)}$ calculation in the Appendix.

In the course of this study we accumulated a wealth of two-point correlator data at finite momentum. This enabled us to compare lattice results for dispersion relations and leptonic decays of finite momentum heavy mesons with continuum expectations. We found that momentum dependent discretization errors were under control and less than 10% up to

about $a_s p \approx 2$. Discretization errors at high momenta in three-point functions have not been critically assessed to date. However, assuming a situation similar to the one found with the two-point functions, prospects for simulating hadrons in semi-leptonic decays with momenta as high as $1.5 - 2 GeV$ look promising. Only slightly finer lattices ($a_s^{-1} \geq 1 GeV$) than those of the present work may be required. This would have to be coupled with an anisotropy of $\chi \approx 2.5$ or higher in order to be able to extract a signal at those high momenta. The experience gained in the present work will be indispensable when picking optimal simulation parameters in the future and going onto more realistic calculations.

ACKNOWLEDGMENTS

This work was supported by the DOE under DE-FG02-91ER40690, PPARC under PPA/G/0/1998/00559 and by NSF. Simulations were carried out at the Ohio Supercomputer Center and at NERSC. We thank Mark Alford for help in checking the gauge and the D234 inversion codes and Peter Boyle for useful discussions on code improvements.

S.C. acknowledges a fellowship from the Royal Society of Edinburgh. J.S. thanks Cornell University and the University of Glasgow for their hospitality during the initial stages of this project. Support from a PPARC Visiting Fellowship PPA/V/S/1997/00666 is gratefully acknowledged.

APPENDIX A: TREE-LEVEL WAVE FUNCTION RENORMALIZATION FOR D234 QUARK ACTIONS

In this appendix we sketch the derivation of the tree-level wave function renormalisations, $Z_q^{(0)}$, for the light quark actions used in this article. Results for $\mathcal{S}_{D234}^{(aniso)}$ have already appeared in reference [18]. One starts from the requirement that the propagator for a zero momentum quark have the form,

$$\begin{aligned} G(t, \vec{p} = 0) &= \int_{-\pi/a_t}^{\pi/a_t} \frac{dp_0}{2\pi} e^{ip_0 t} \overline{G}(p_0, \vec{p} = 0) \\ &\equiv Z_q e^{-M_1 t} \frac{1 + \gamma_0}{2} + \dots \end{aligned} \quad (A1)$$

$\overline{G}(p)$ is the momentum space propagator and M_1 denotes the pole mass. The dots refer to lattice artifacts and additional multi-particle states that could be created by the lattice fermion field operator Ψ beyond the single quark state. Writing

$$\frac{1}{a_t} \overline{G}(p_0, \vec{p} = 0) = \frac{1}{i\gamma_0 A + B}, \quad (A2)$$

and using the complex variable

$$z \equiv e^{ia_t p_0} = e^{-a_t E}, \quad (A3)$$

one finds

$$G(t, \vec{p} = 0) = \int_{-\pi/a_t}^{\pi/a_t} \frac{dp_0}{2\pi} e^{ip_0 t} a_t \frac{-i\gamma_0 A + B}{(A^2 + B^2)} = \int \frac{dz}{2\pi i z} z^{t/a_t} \frac{-i\gamma_0 A + B}{(A + iB)(A - iB)}. \quad (\text{A4})$$

One can show that the pole,

$$z_1 \equiv e^{-a_t M_1} \quad (\text{A5})$$

corresponding to a physical positive energy particle obeys $(A - iB)|_{z=z_1} = 0$ or $B|_{z=z_1} = -iA|_{z=z_1}$. The contribution to $G(t, 0)$ from the residue at this physical pole is then given by,

$$\left[\frac{z^{t/a_t} (-i\gamma_0 A + B)}{z \frac{d}{dz} (A^2 + B^2)} \right]_{z=z_1} = \frac{(\gamma_0 + 1)}{2} e^{-M_1 t} \left[\frac{-i}{z(A' - iB')} \right]_{z=z_1}. \quad (\text{A6})$$

Using

$$\left(z \frac{df}{dz} \right)_{z=z_1} = -i \left(\frac{df}{d(a_t p_0)} \right)_{p_0=iM_1}. \quad (\text{A7})$$

and comparing with eq.(A1), one finds,

$$Z_q = \left[\frac{1}{\frac{d}{d(a_t p_0)} (A - iB)} \right]_{p_0=iM_1}. \quad (\text{A8})$$

For $\mathcal{S}_{D234}^{(aniso)}$ one has at tree-level,

$$A^{(aniso)} = \sin(a_t p_0) \quad (\text{A9})$$

$$B^{(aniso)} = a_t m + \chi - \chi \cos(a_t p_0) \quad (\text{A10})$$

$$(\text{A11})$$

and

$$e^{-a_t M_1} = \frac{(a_t m + \chi) - \sqrt{(a_t m + \chi)^2 + 1 - \chi^2}}{\chi - 1} \quad (\text{A12})$$

or equivalently,

$$e^{a_t M_1} = \frac{(a_t m + \chi) + \sqrt{(a_t m + \chi)^2 + 1 - \chi^2}}{\chi + 1}. \quad (\text{A13})$$

As explained in reference [18] $m = m_0 - m_c$ and m_c is the value of m_0 that gives a massless pion. From eq.(A8) one finds,

$$Z_q^{(0),aniso} = \frac{1}{\cosh(a_t M_1) + \chi \sinh(a_t M_1)} = \frac{1}{\sqrt{(a_t m)^2 + 2(a_t m)\chi + 1}}. \quad (\text{A14})$$

For the isotropic action $\mathcal{S}_{D234}^{(iso)}$ with higher time derivatives the formulas are more complicated.

$$A^{(iso)} = \frac{4}{3}\sin(a_t p_0) - \frac{1}{6}\sin(2a_t p_0) \quad (\text{A15})$$

$$B^{(iso)} = a_t m + \frac{4}{3}(1 - \cos(a_t p_0)) - \frac{1}{6}\sin^2(a_t p_0). \quad (\text{A16})$$

Eq(A8) leads to

$$Z_q^{(0),iso} = \frac{1}{\left[\frac{4}{3}e^{a_t M_1} - \frac{1}{3}(\cosh^2(a_t M_1) + \sinh^2(a_t M_1) + \sinh(a_t M_1)\cosh(a_t M_1))\right]}. \quad (\text{A17})$$

The tree-level physical pole $z_1 = e^{-a_t M_1}$ is the solution to,

$$z^4 - (24a_t m + 30)z^2 + 32z - 3 = 0 \quad (\text{A18})$$

that evolves smoothly from $z_1 = 1$ at $a_t m = 0$. A lengthy closed expression for z_1 as a function of $a_t m$ can be obtained (using for instance Mathematica), however we do not consider it worthwhile reproducing it here. It is easier to plug in specific values for $a_t m$ into eq.(A18) before solving for the roots. At small $a_t m$ the physical pole is well approximated by

$$\frac{1}{z_1} = e^{a_t M_1} = 1 + (a_t m) + \frac{1}{6}(a_t m)^3 - \frac{5}{24}(a_t m)^4 + O((a_t m)^5). \quad (\text{A19})$$

For the mass parameter values used in the current simulations, the sum of just the first three terms in (A19) differs from the exact solution to eq.(A18) by only 1%.

In order to get explicit values for $Z_q^{(0)}$, one needs to know $a_t m = a_t(m_0 - m_c)$. Since we have data at only one light quark mass, we do not have a nonperturbative estimate for $a_t m_c$ based on a vanishing pion mass. We approximate $a_t m_c$ using perturbation theory and find [18], $a_t m \approx 0.635$ and $a_t m \approx 0.196$ respectively for the isotropic and anisotropic lattices. This leads to

$$\sqrt{Z_q^{(0),iso}} = \frac{1}{1.2226} \quad (\text{A20})$$

$$\sqrt{Z_q^{(0),aniso}} = \frac{1}{1.3286} \quad (\text{A21})$$

which are the values used in section IV.

REFERENCES

- [1] G.P. Lepage, Nucl. Phys. **B** (Proc. Suppl.)**60A** 267 (1998).
- [2] C. Morningstar and M. Peardon, Phys. Rev.**D60**:034509 (1999).
- [3] T. Manke *et al.*, Phys. Rev. Lett **82**:4396 (1999).
- [4] I. Drummond *et al.*, Phys. Lett. **B478**, 151 (2000).
- [5] CP-PACS Collaboration, T. Manke *et al.*, Nucl. Phys. **B**(Proc. Suppl.)**83**, 319 (2000).
- [6] F. Karsch, Nucl. Phys. **B205** [FS5], 285 (1982).
- [7] S. Sakai, T. Saito and A. Nakamura, Nucl. Phys. **B584**, 528 (2000).
- [8] T.R. Klassen, Nucl. Phys. **B**(Proc. Suppl.)**73**, 918 (1999).
- [9] P. Chen, hep-lat/0006019 ; P. Chen *et al.*, hep-lat/0010069.
CP-PACS Collaboration, A. Ali Khan *et al.*, hep-lat/0011005.
- [10] For recent studies on the lattice see:
S.Hashimoto *et al.* Phys. Rev. **D58**:014502 (1998); T. Onogi, hep-lat/0011008;
K.C. Bowler *et al.* [UKQCD Collaboration], Phys. Lett. **B486** (2000) 111;
A. Abada *et al.* , hep-lat/0011065 ;
S.M. Ryan *et al.*, Nucl. Phys. Proc. Suppl. **83** (2000) 328 ; A. El-Khadra *et al.*, hep-ph/0101023.
- [11] P. Weisz; Nucl. Phys. **B212** 1 (1983); P. Weisz and R. Wohlert, Nucl. Phys. **B236** 397 (1984) ; erratum, *ibid.* **B247** 544 (1984).
- [12] M. Alford, T. Klassen and G. P. Lepage, Phys. Rev. **D58**:034503 (1998), Nucl. Phys. **B496** 377 (1997).
- [13] G.P. Lepage *et al.*, Phys. Rev. **D46**, 4052 (1992).
- [14] S. Naik, Nucl. Phys. **B316**, 238 (1989).
G. P. Lepage, Phys. Rev. **D59**:074501 (1999).
K. Orginos, D. Toussaint and R.L. Sugar, Phys. Rev. **D60**:054503 (1999).
- [15] A. El-Khadra, A. Kronfeld and P. Mackenzie, Phys. Rev. **D55**, 3933 (1997).
- [16] G.P. Lepage and P.B. Mackenzie, Phys. Rev. **D48**, 2250 (1993).
- [17] M. Alford *et al.*, hep-lat/0003019.
- [18] S. Groote and J. Shigemitsu, Phys. Rev. **D62**:014508 (2000).
- [19] I. Drummond *et al.*, Nucl. Phys. **B**(Proc. Suppl.)**73**, 336 (1999).
- [20] J. Sloan, private communication.
- [21] J. Hein *et al.*, Phys. Rev. **D62**:074503 (2000).
- [22] S. Collins *et al.*, Phys. Rev. **D63**:034505 (2001).
- [23] J.N. Simone, Nucl. Phys. **B**(Proc. Suppl.) **53**, 386 (1997).
- [24] S. Collins *et al.*, in preparation.
- [25] A. Ali Khan *et al.*, Phys. Rev. **D62**:054505 (2000).
- [26] R. Lewis and R. Woloshyn, Phys. Rev. **D58**:074506 (1998) ; *ibid.* **D62**:114507 (2000).
- [27] P. Boyle (UKQCD collaboration), Nucl. Phys. **B**(Proc. Suppl.) **63**, 314 (1998).
- [28] P.B. Mackenzie, S. Ryan and J. Simone, Nucl. Phys. **B**(Proc. Suppl.) **63**, 305 (1998).
- [29] K-I. Ishikawa *et al.* (JLQCD collaboration), Phys. Rev. **D61**:074501 (2000).
- [30] C. Morningstar and J. Shigemitsu; Phys. Rev. **D59**:094504 (1999).
- [31] D. Kaplan, Phys. Lett. **B288**, 342 (1992).
R. Narayanan and H. Neuberger, Phys. Lett. **B302**, 62 (1993).
Y. Shamir, Nucl. Phys. **B406**, 90 (1993).

- [32] R. Frezzotti *et al.*, Nucl. Phys. **B**(Proc. Suppl.) **83**, 941 (2000).
- [33] G.P. Lepage, Lectures given at TASI '89, Boulder, Colorado, 1989.
- [34] CLEO Collaboration: A. Bean *et al.*, Phys. Lett. **B317**, 647 (1993); J.Bartelt *et al.*, Phys. Lett. **B405**, 373 (1997).

TABLES

TABLE I. Simulation Details.

	isotropic	anisotropic
lattice size	$8^3 \times 20$	$8^3 \times 48$
# configs	200	200
β	1.719	1.8
Landau link u_0	0.797 [12]	$u_s=0.721$ $u_t=0.992$ [17]
χ_0		6.0
$\chi = a_s/a_t$	1	5.3 [17]
C_0	1	0.82
a_s^{-1}	0.8(1) GeV	0.7(1) GeV
a_t^{-1}	0.8(1) GeV	3.7(4) GeV
$a_t m_0$	1.15	0.39
P/V	0.725(5)	0.726(6)
typical # of BiCGstab iters	140 - 160	220 - 270
$a_s M_0$	6.5	7.0 and 2.0

TABLE II. Some Spectrum Results. The first errors are statistical and the second are estimates for errors due to uncertainties in the scale. The hyperfine splittings have not been adjusted for incomplete tuning of the heavy quark mass (see text for adjusted numbers).

	isotropic	anisotropic	Experiment
light-light			
“pion” mass	0.856(3)(86) GeV	0.840(7)(84) GeV	
“rho” mass	1.179(10)(118) GeV	1.158(7)(116) GeV	
heavy-light			
B_s	5.65(31)(57) GeV	4.80(20)(48) GeV	5.369 GeV
D_s		2.04(5)(20) GeV	1.969 GeV
$B_s^* - B_s$	46(3)(5) MeV	45(2)(5) MeV	47.0(26) MeV
$D_s^* - D_s$		143(4)(14) MeV	143.8(4) MeV

FIGURES

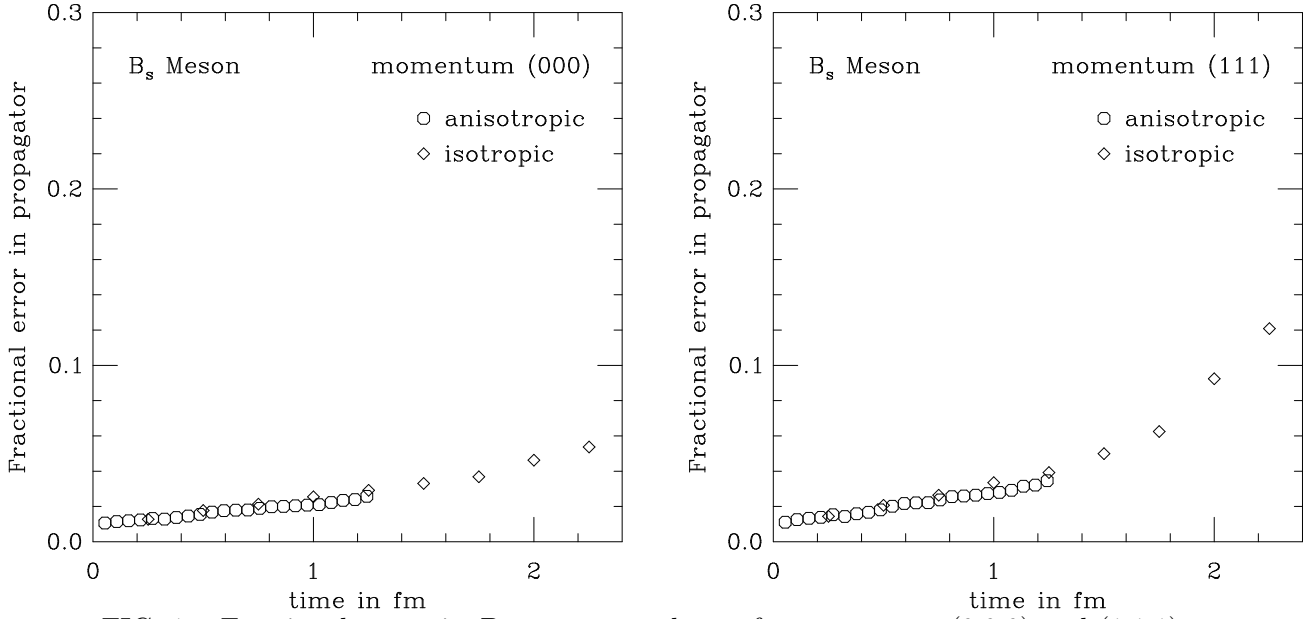


FIG. 1. Fractional errors in B_s meson correlators for momentum $(0,0,0)$ and $(1,1,1)$.

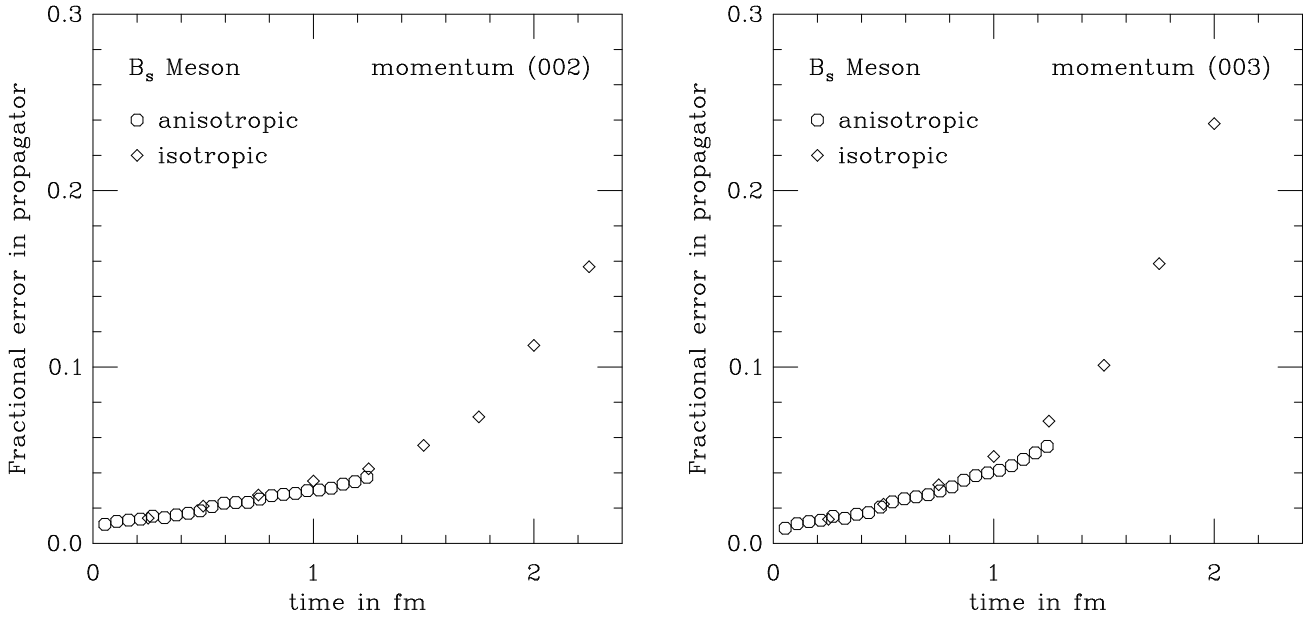


FIG. 2. Fractional errors in B_s meson correlators for momentum $(0,0,2)$ and $(0,0,3)$.

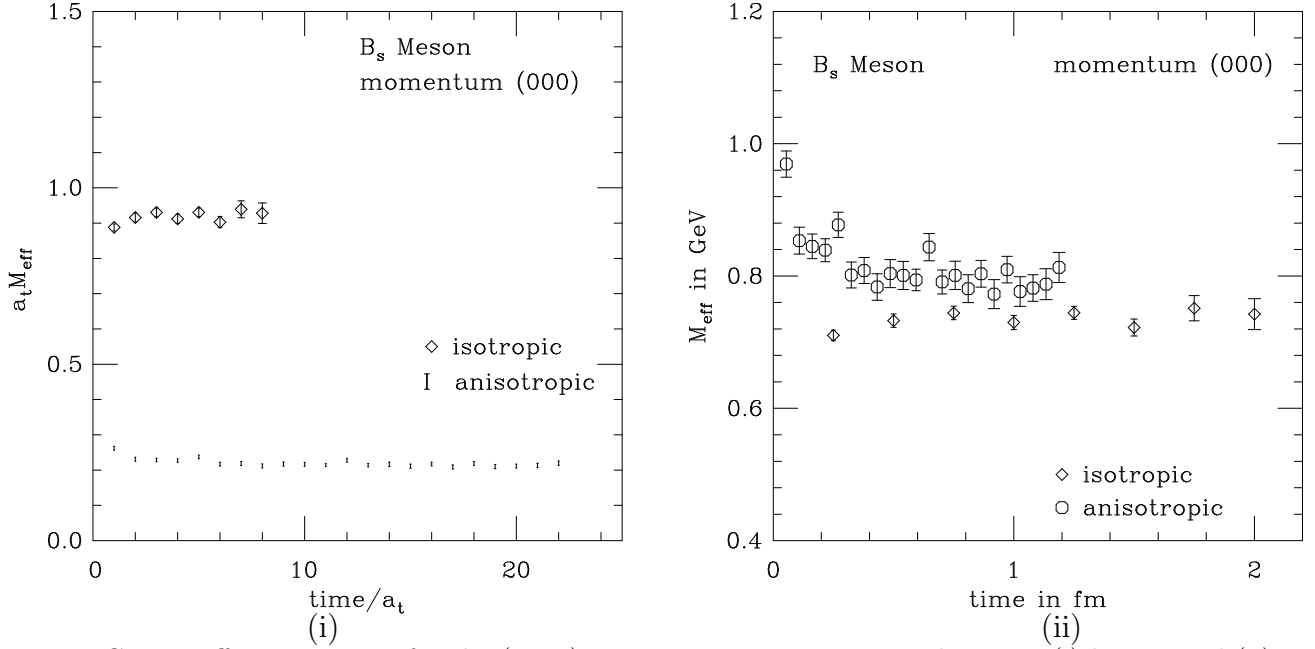


FIG. 3. Effective masses for the (0,0,0) momentum B_s meson correlators in (i) lattice and (ii) physical units.

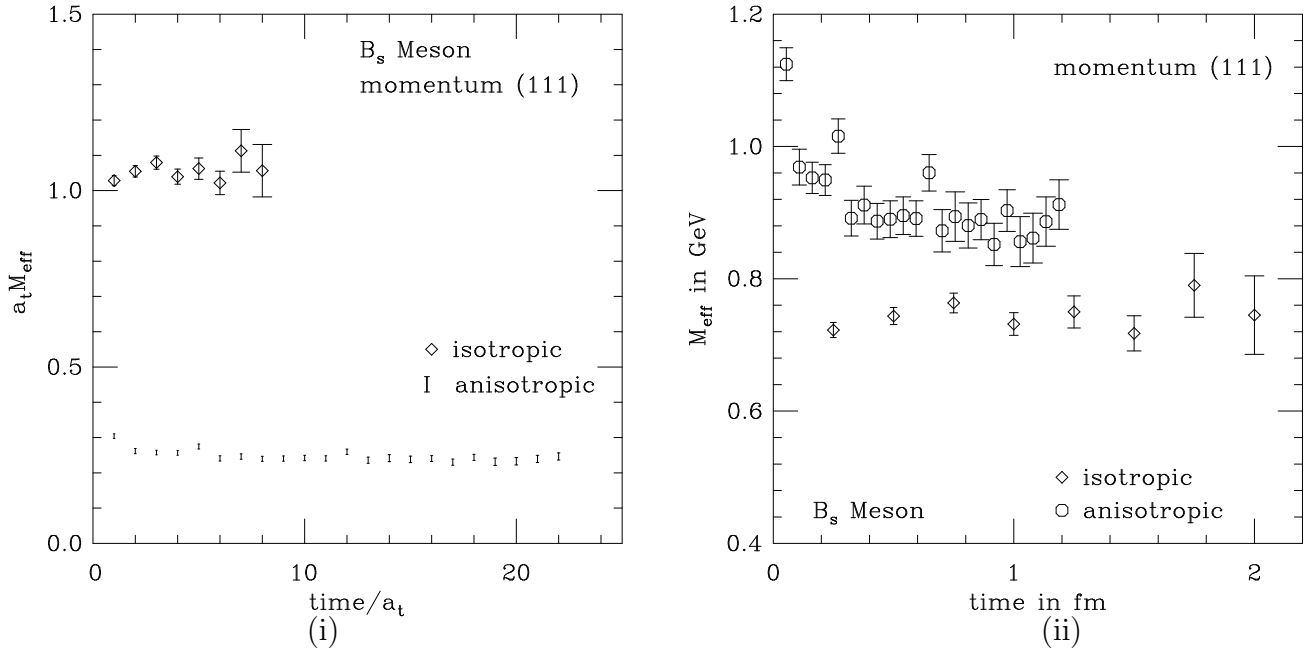


FIG. 4. Effective masses for the (1,1,1) momentum B_s meson correlators in (i) lattice and (ii) physical units. The isotropic points in (ii) have been shifted down for clarity.

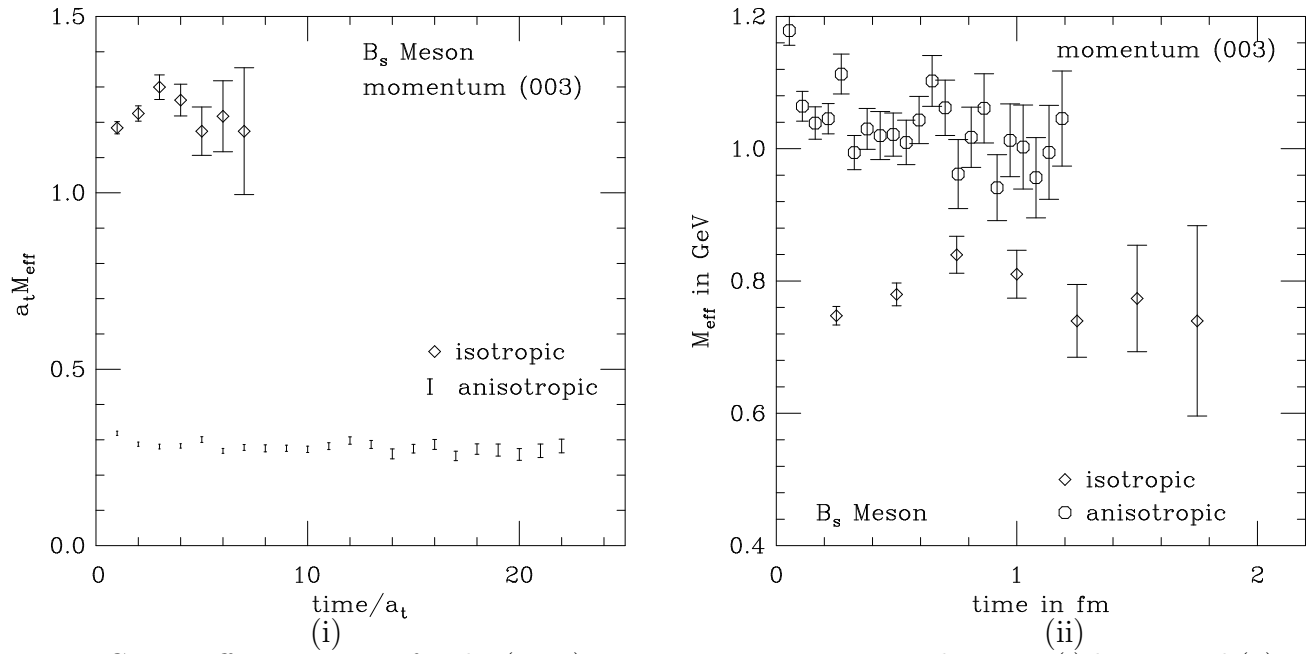


FIG. 5. Effective masses for the (0,0,3) momentum B_s meson correlators in (i) lattice and (ii) physical units. The isotropic points in (ii) have been shifted down for clarity.

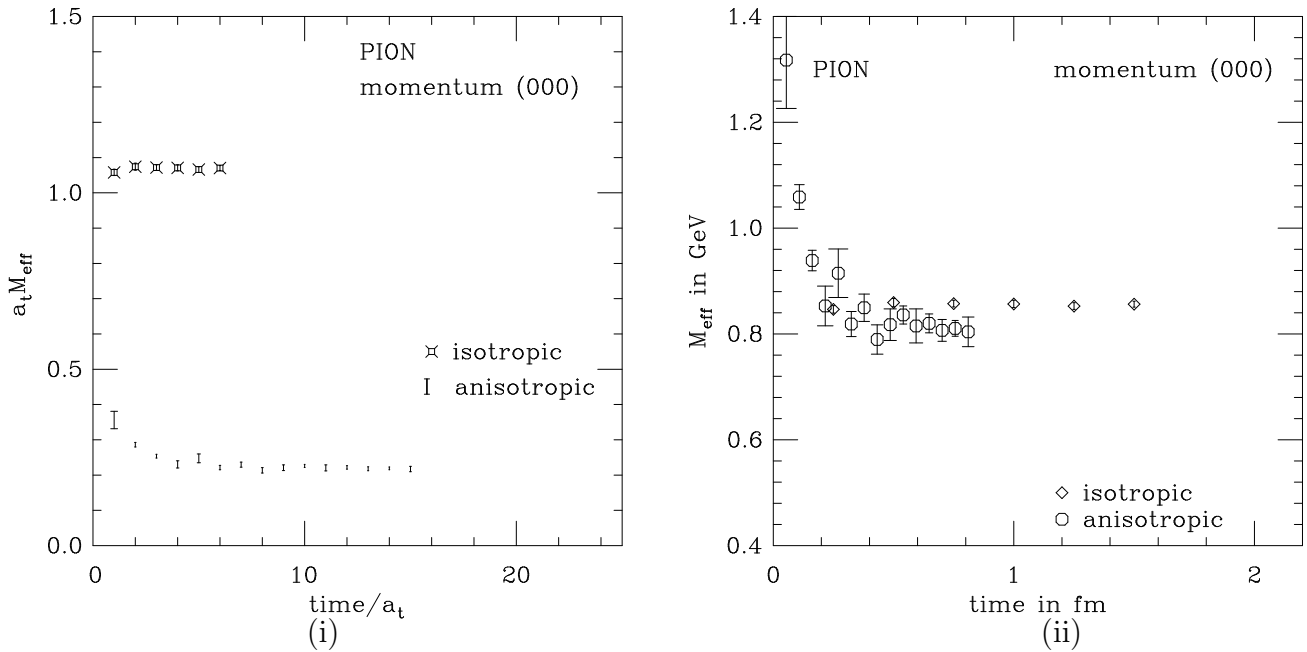


FIG. 6. Effective masses for the (0,0,0) momentum pion correlators in (i) lattice and (ii) physical units.

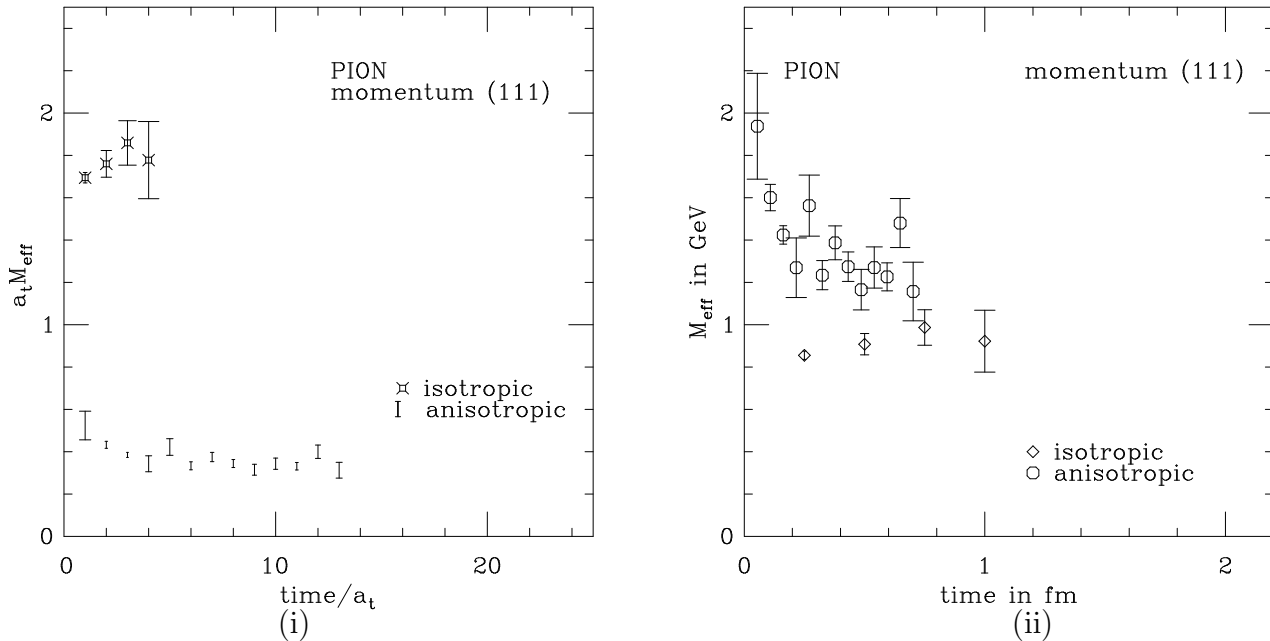


FIG. 7. Effective masses for the (1,1,1) momentum pion correlators in (i) lattice and (ii) physical units. The isotropic points in (ii) have been shifted down for clarity.

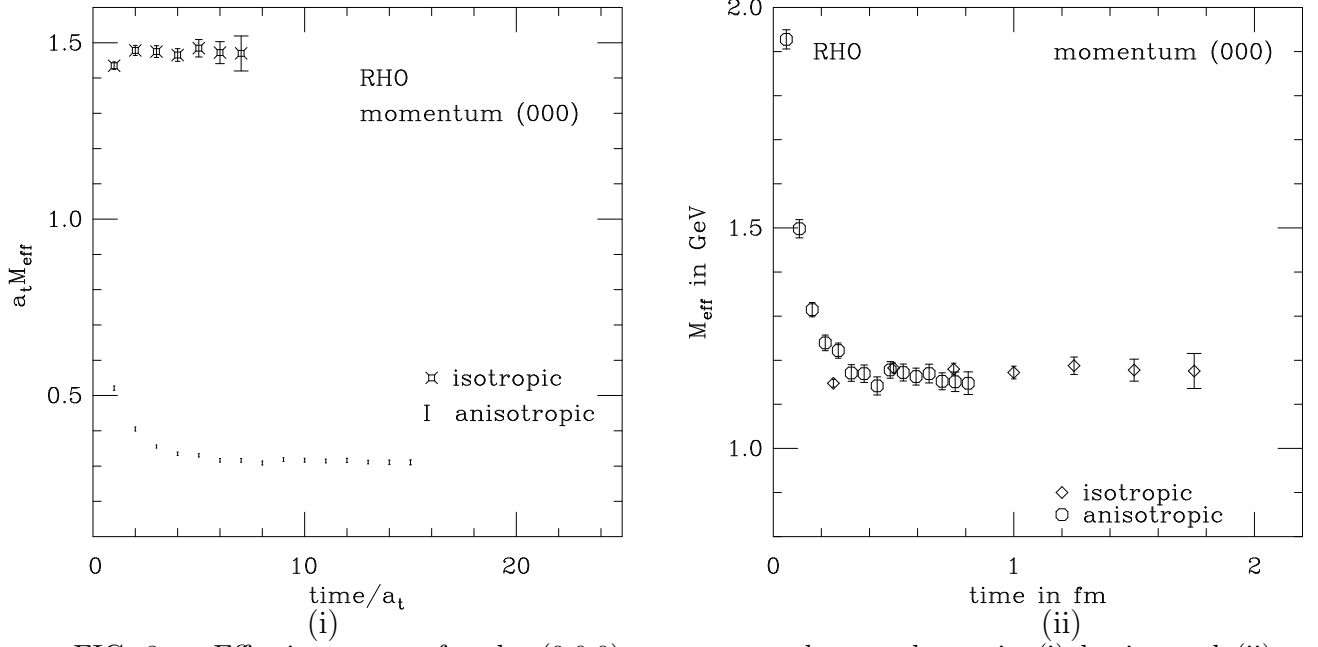


FIG. 8. Effective masses for the (0,0,0) momentum rho correlators in (i) lattice and (ii) physical units.

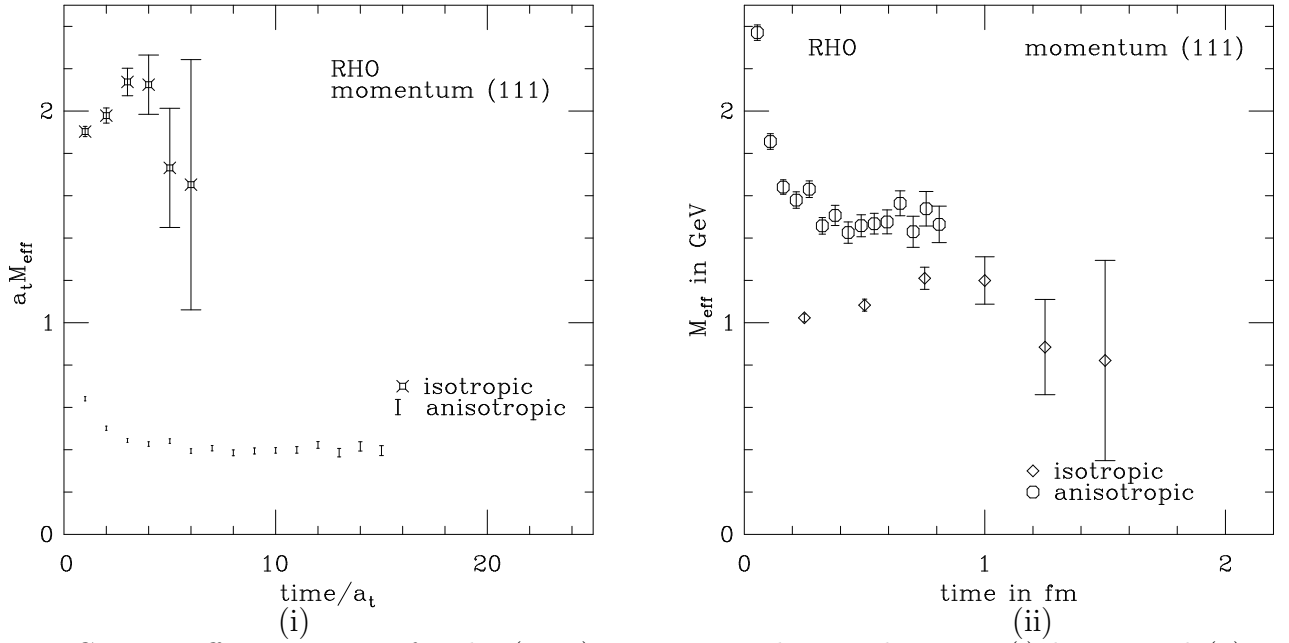


FIG. 9. Effective masses for the (1,1,1) momentum rho correlators in (i) lattice and (ii) physical units. The isotropic points in (ii) have been shifted down for clarity.

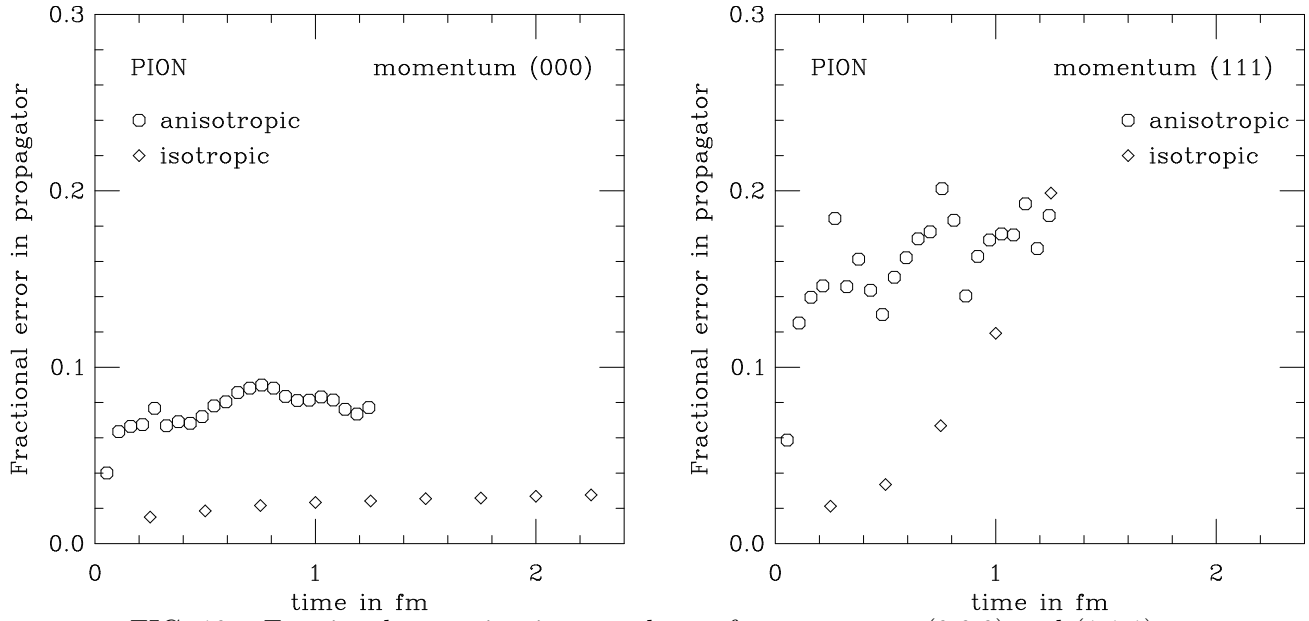


FIG. 10. Fractional errors in pion correlators for momentum $(0,0,0)$ and $(1,1,1)$.

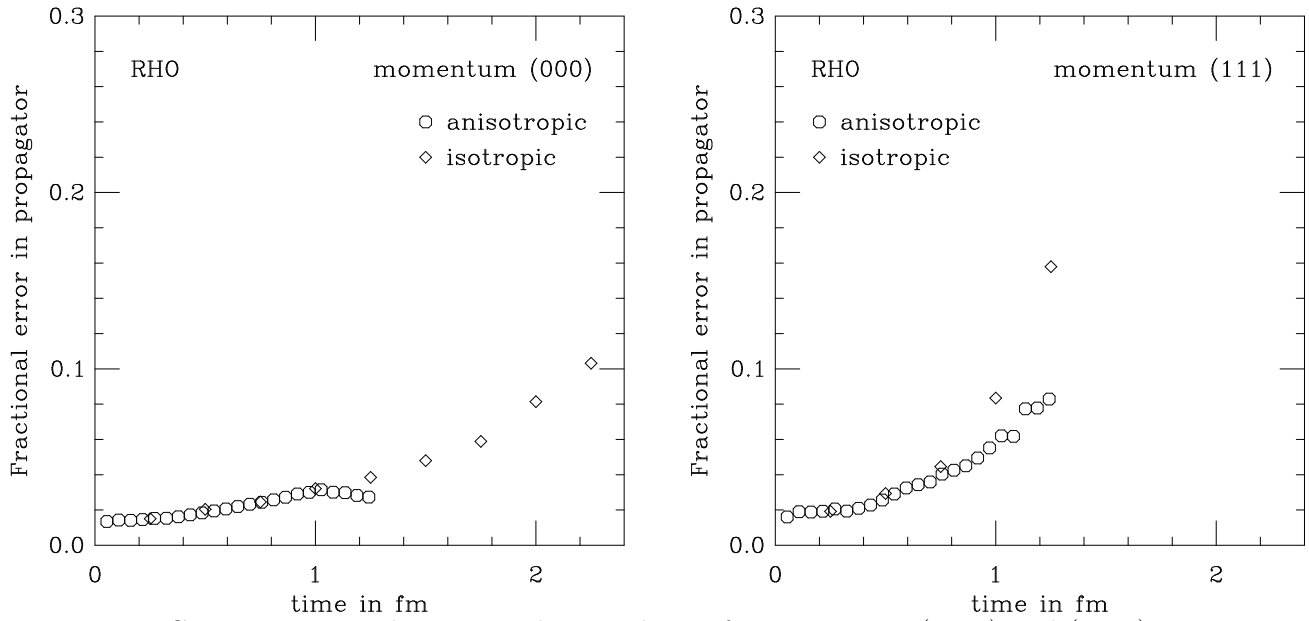


FIG. 11. Fractional errors in rho correlators for momentum $(0,0,0)$ and $(1,1,1)$.

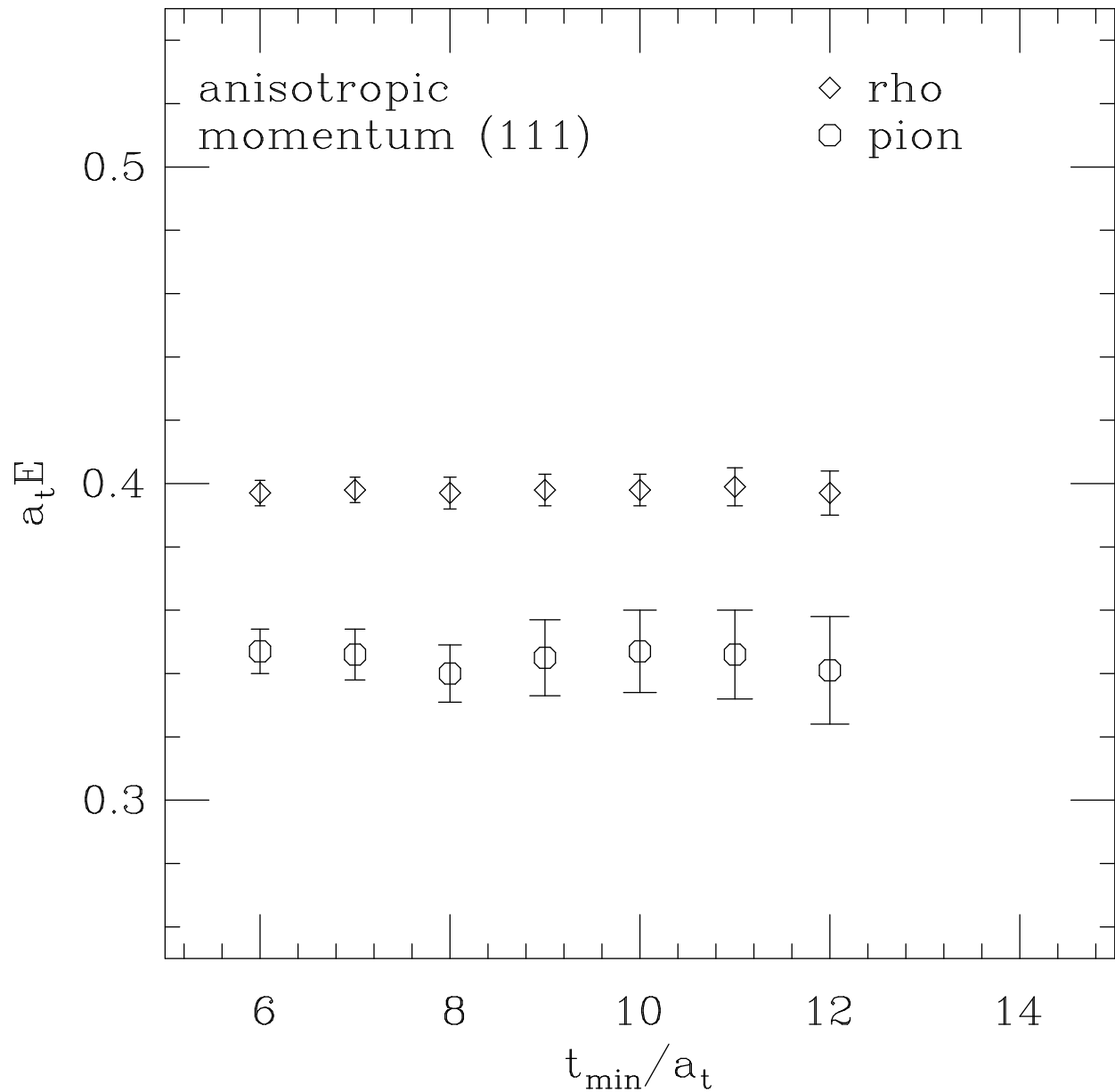


FIG. 12. Fitted energies versus t_{\min}/a_t for the pion and the rho for momentum (1,1,1) on anisotropic lattices. Single cosh fits were used with t_{\max}/a_t fixed at 22. Errors are from a bootstrap over 200 ensembles.

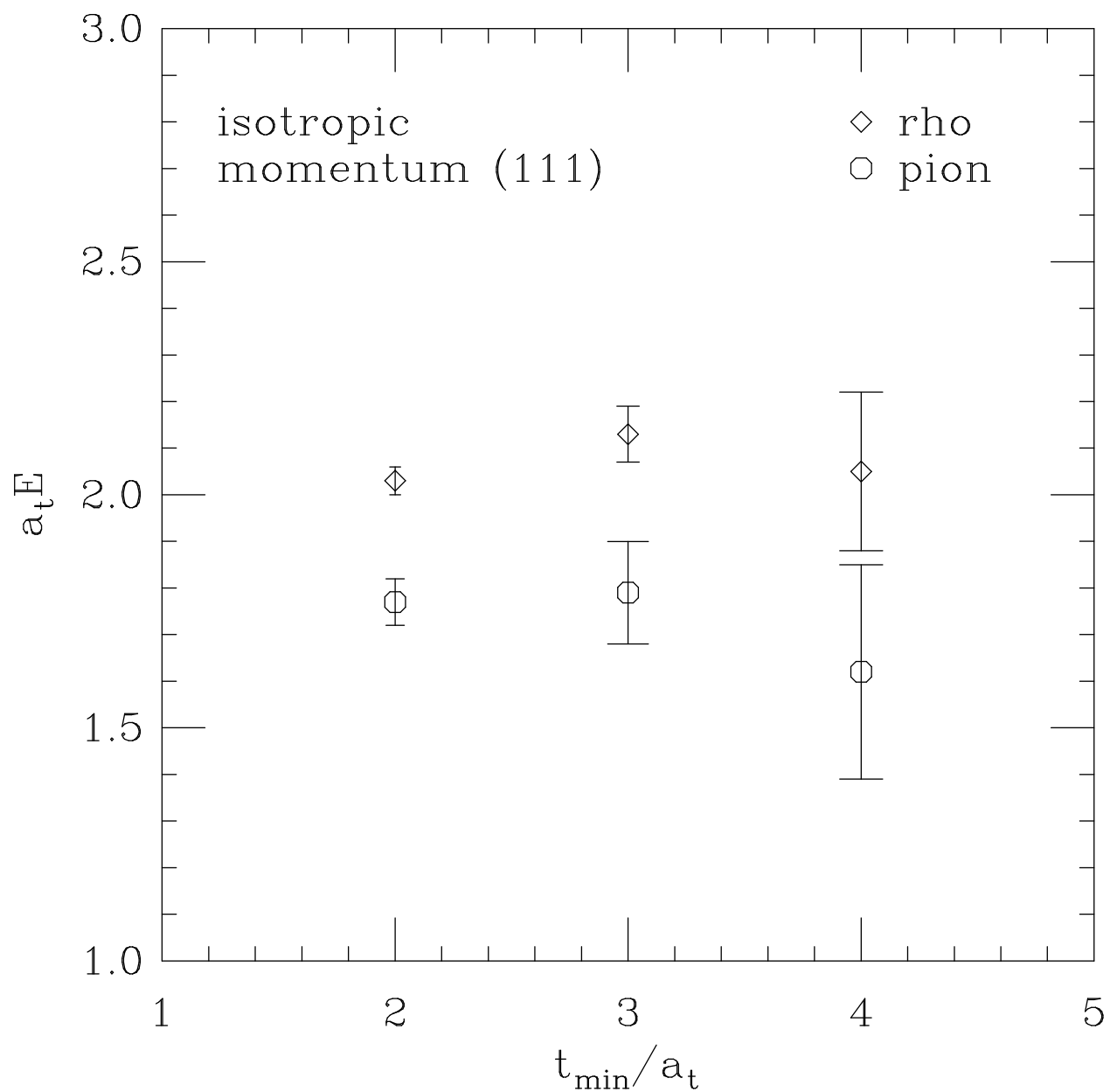


FIG. 13. Fitted energies versus t_{\min}/a_t for the pion and the rho for momentum (1,1,1) on isotropic lattices. Single cosh fits were used with t_{\max}/a_t fixed at 9. Errors are from a bootstrap over 200 ensembles.

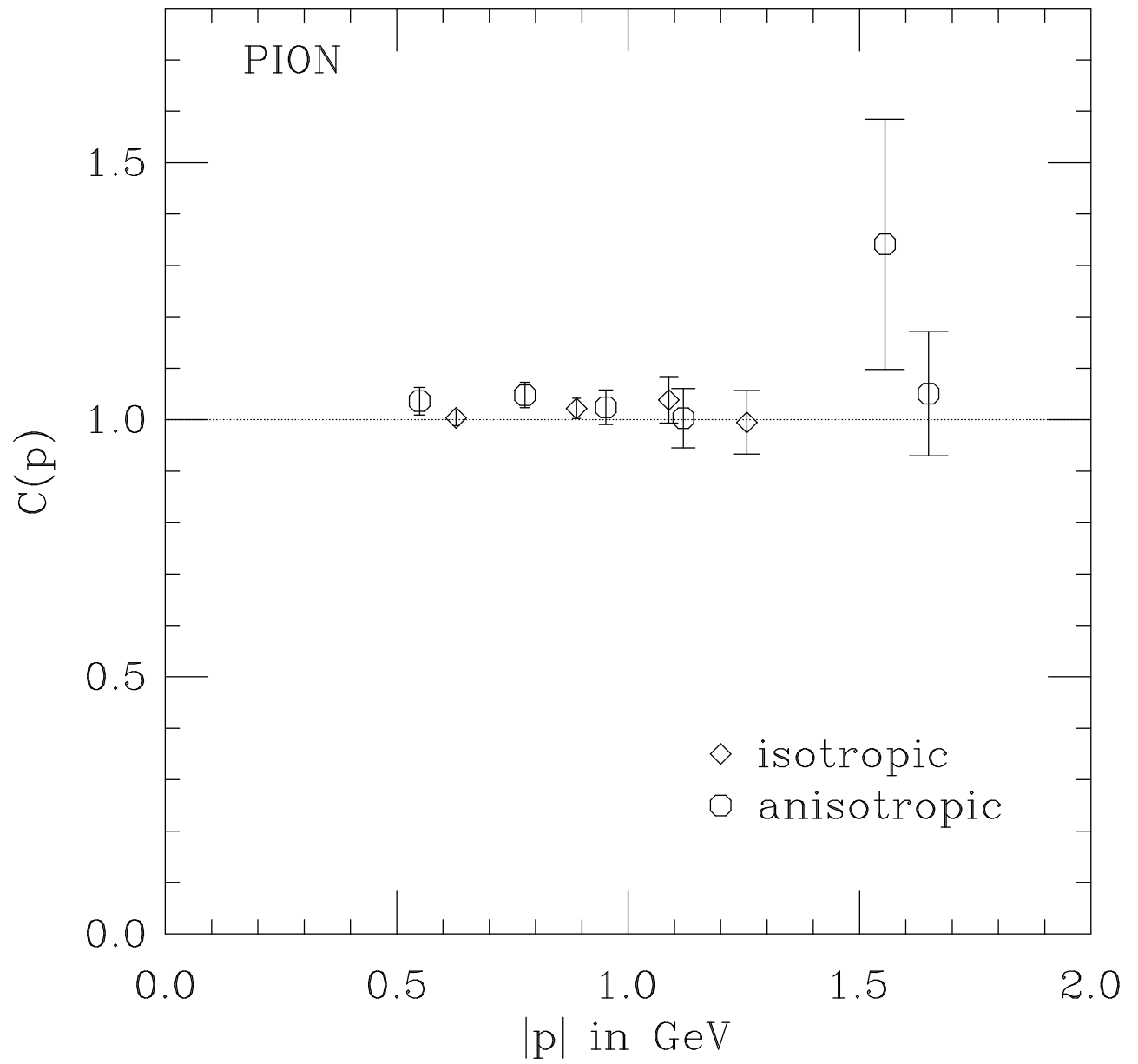


FIG. 14. $C(p)$ versus momentum for the pion.

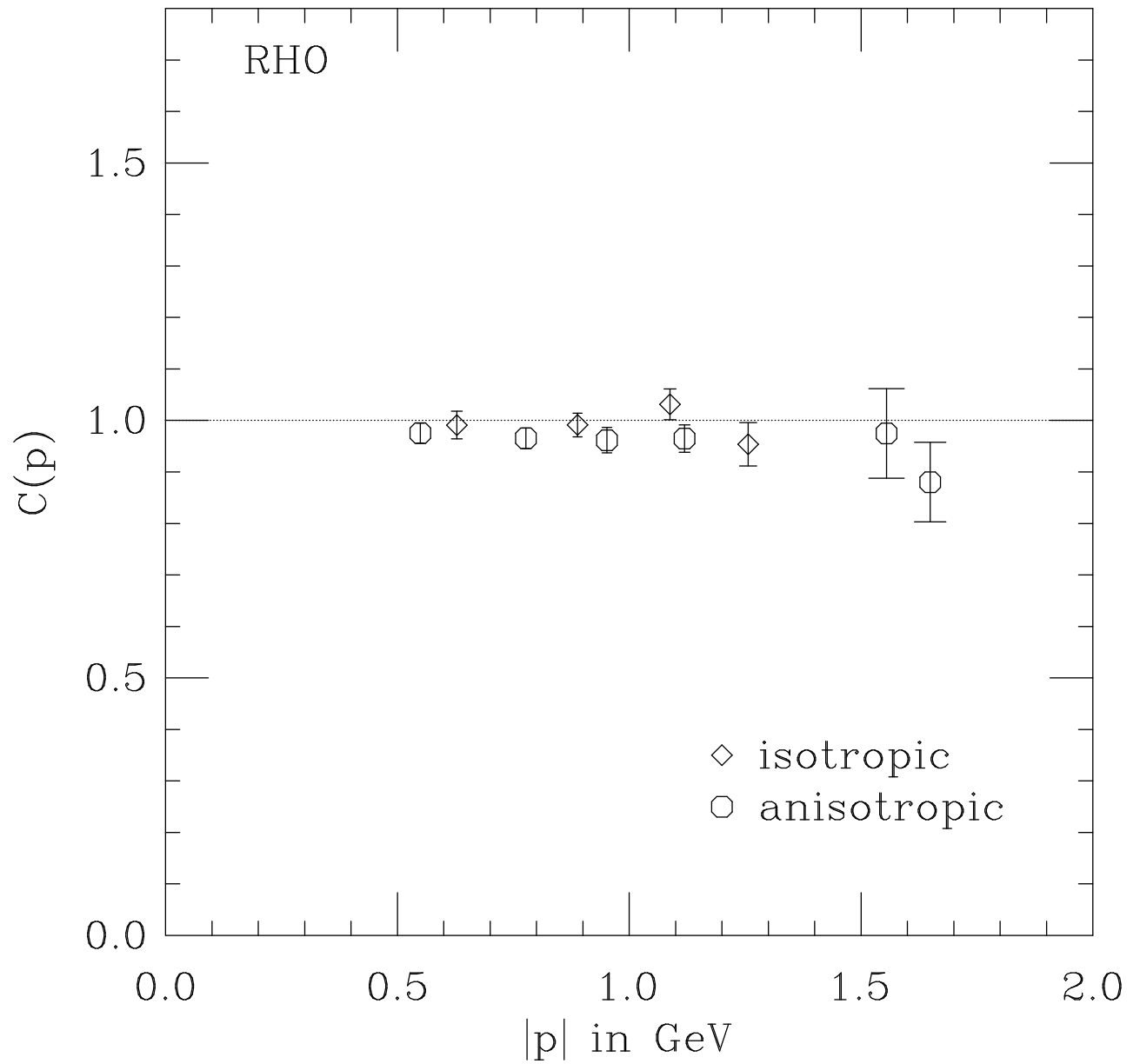
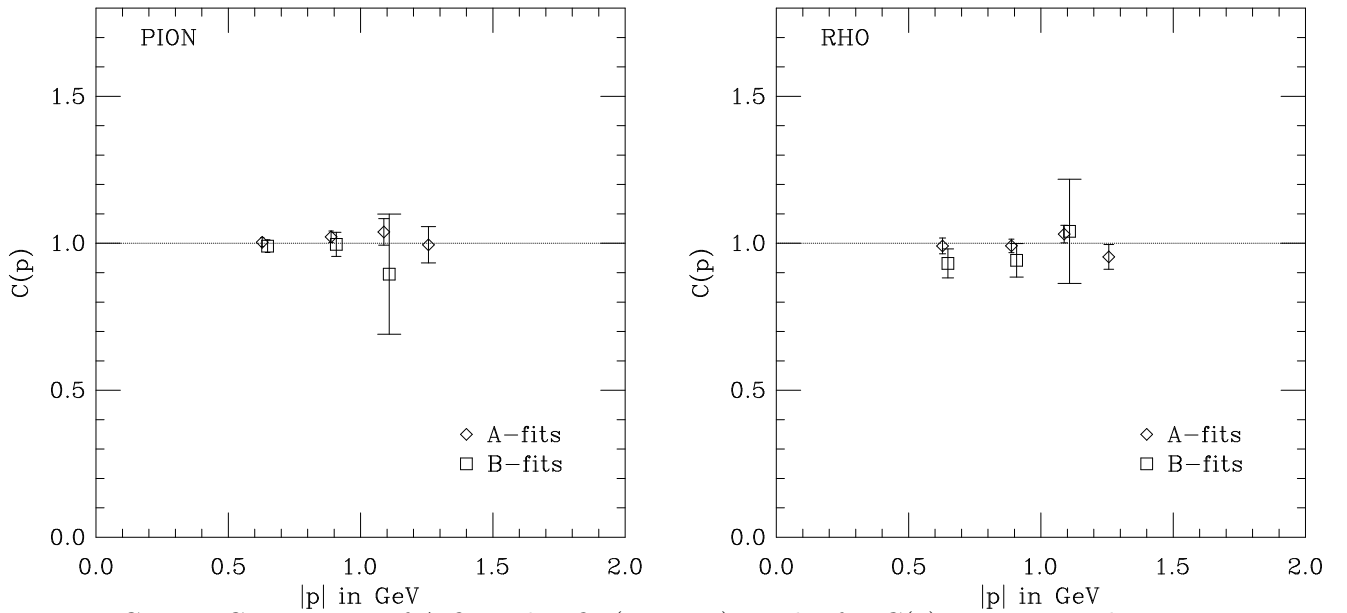
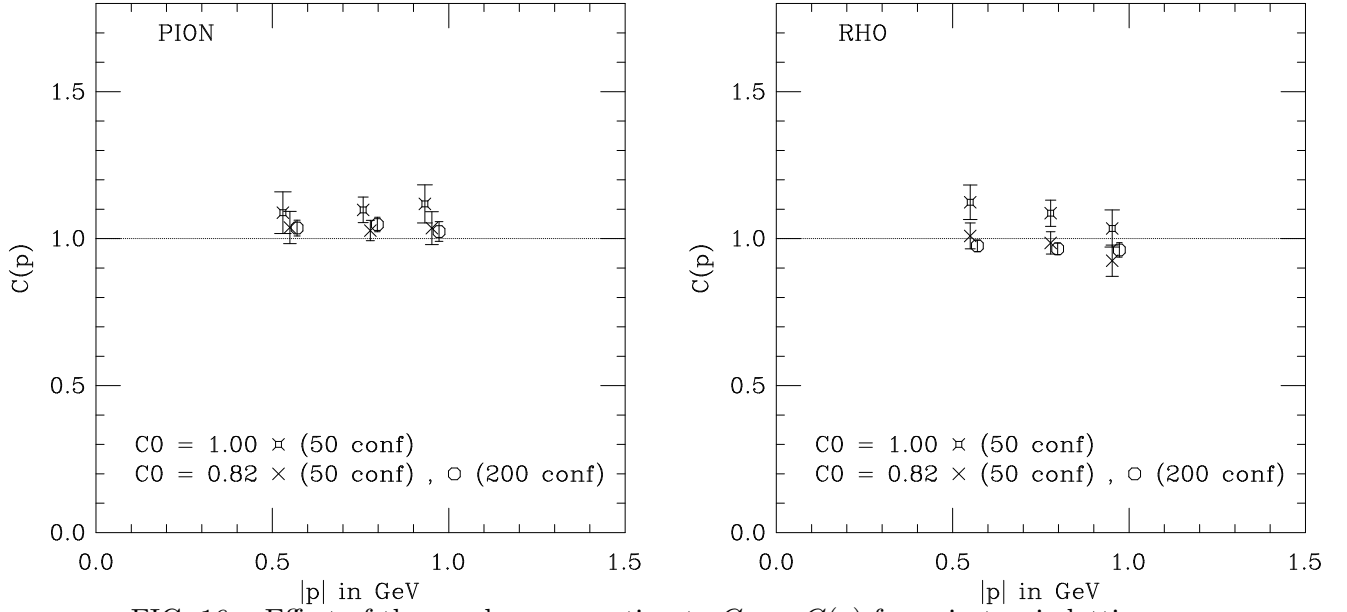


FIG. 15. $C(p)$ versus momentum for the rho.



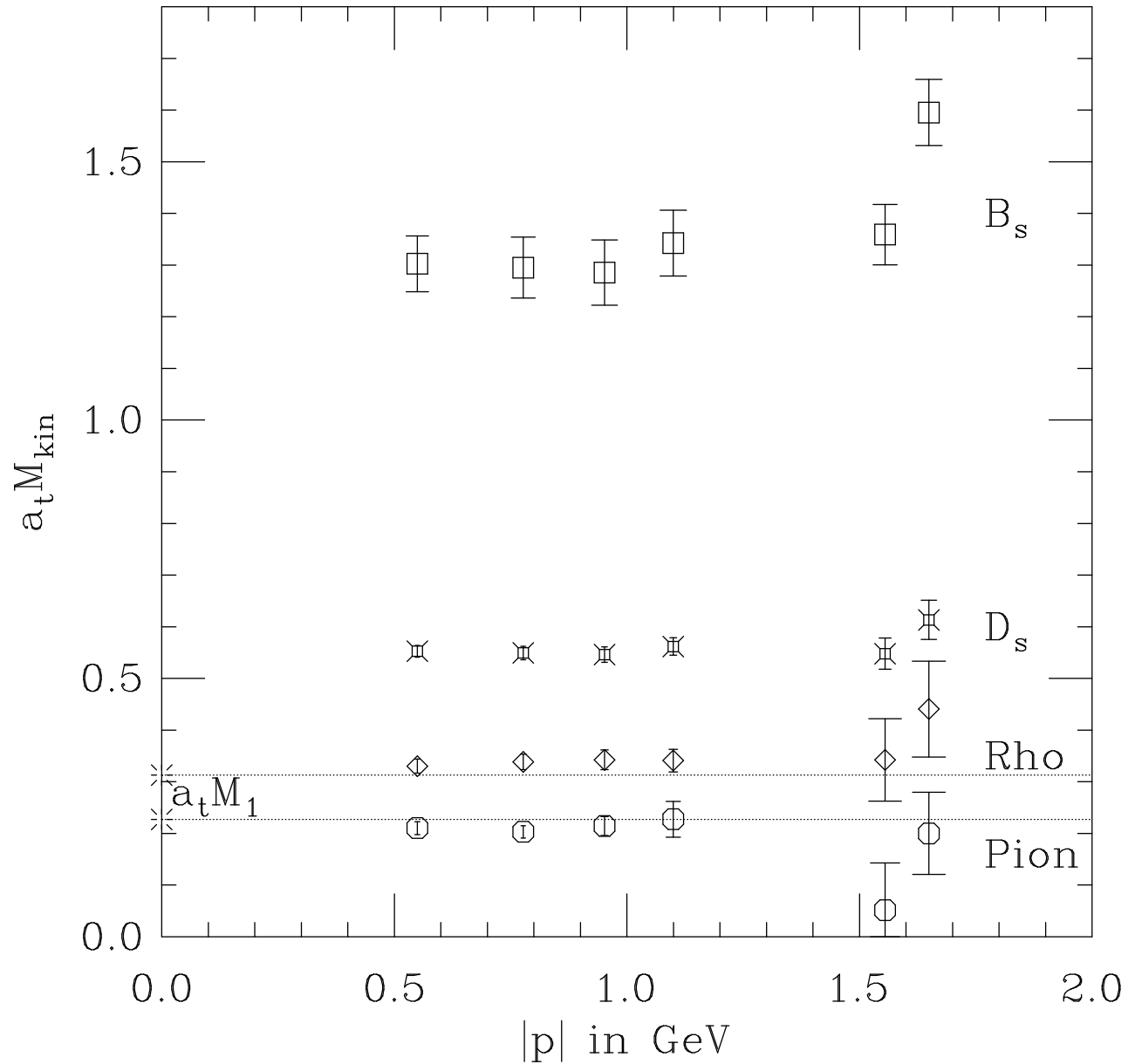


FIG. 18. Kinetic mass in lattice units versus momentum of correlator from which it was extracted for the B_s , D_s , rho and pi mesons. All results are from anisotropic lattices. The horizontal lines show the rest masses $a_t M_1$ for the rho and the pi.

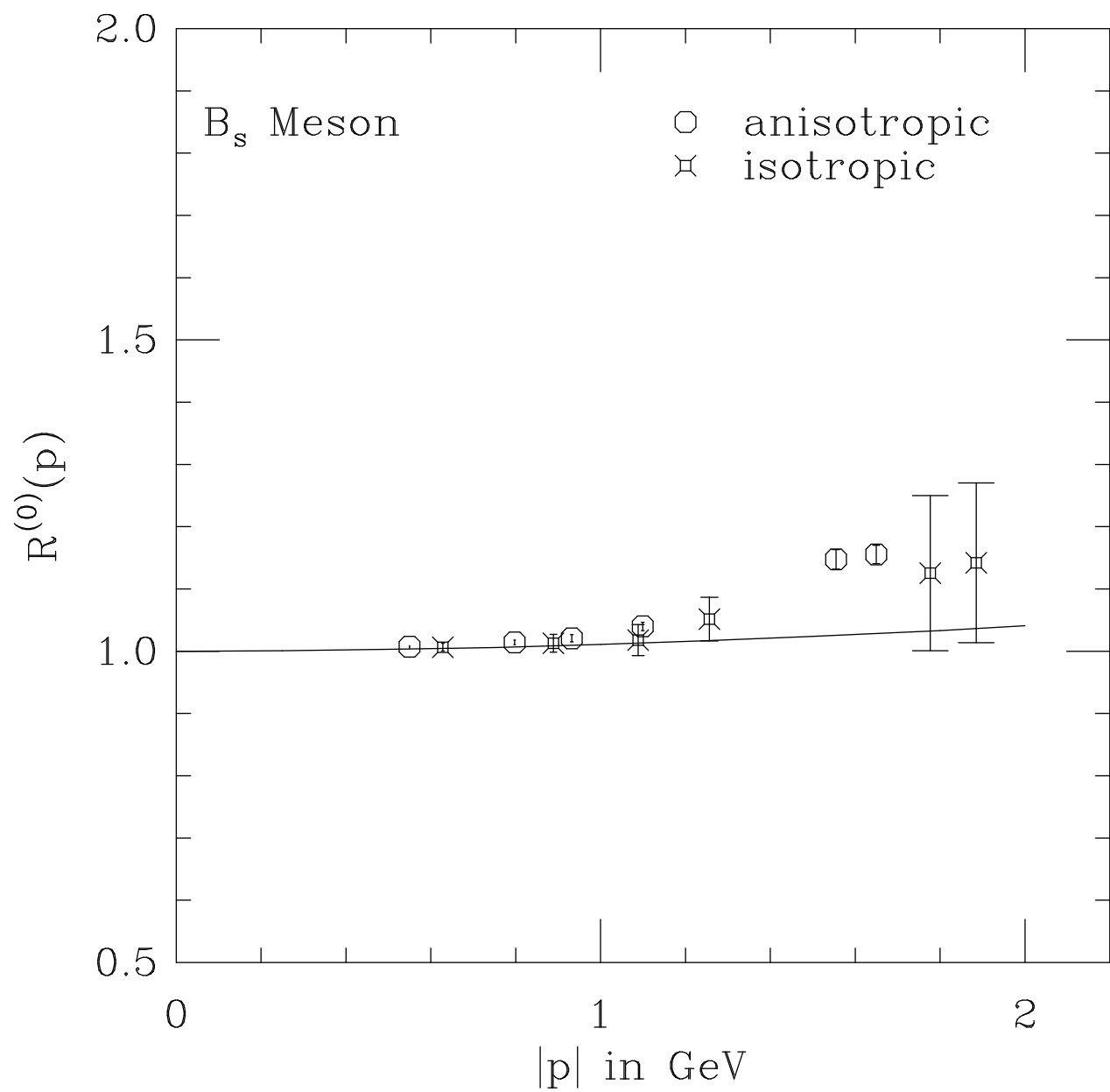


FIG. 19. $R^{(0)}(p)$ as defined in eq.(26) for the B_s meson. The full line shows $\sqrt{E(p)}/\sqrt{M_{PS}}$.

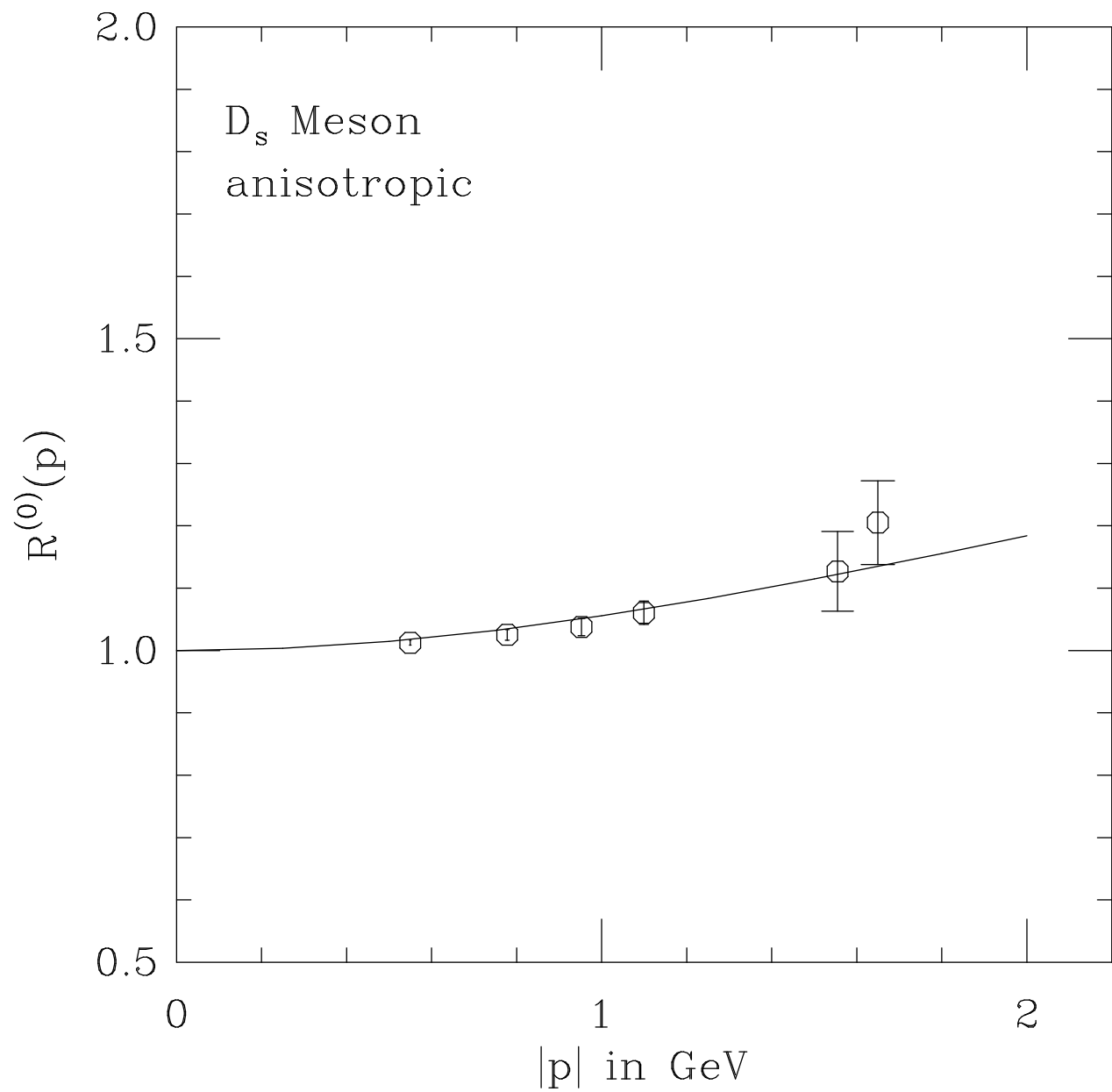


FIG. 20. $R^{(0)}(p)$ as defined in eq.(26) for the D_s meson. The full line shows $\sqrt{E(p)}/\sqrt{M_{PS}}$.

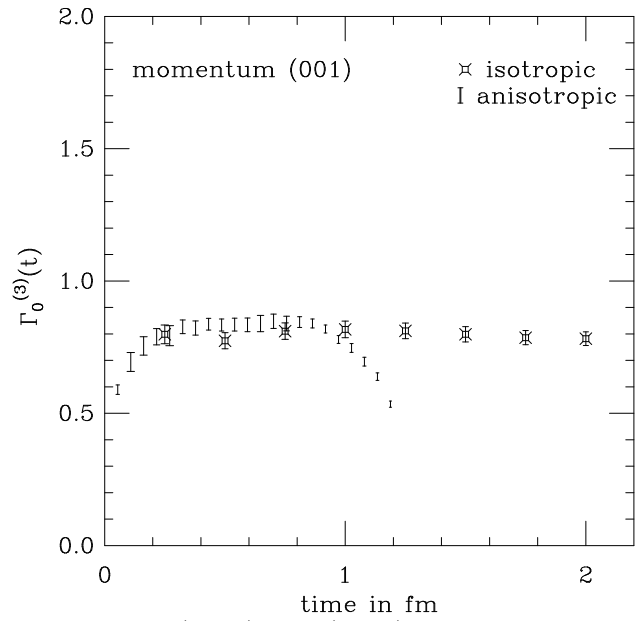
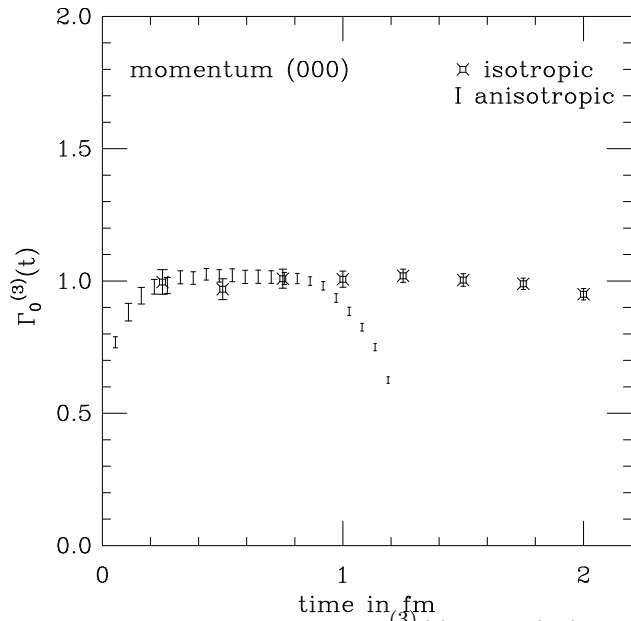


FIG. 21. $\Gamma_0^{(3)}(t)$ of eq.(34) for pion momentum (0,0,0) and (0,0,1).

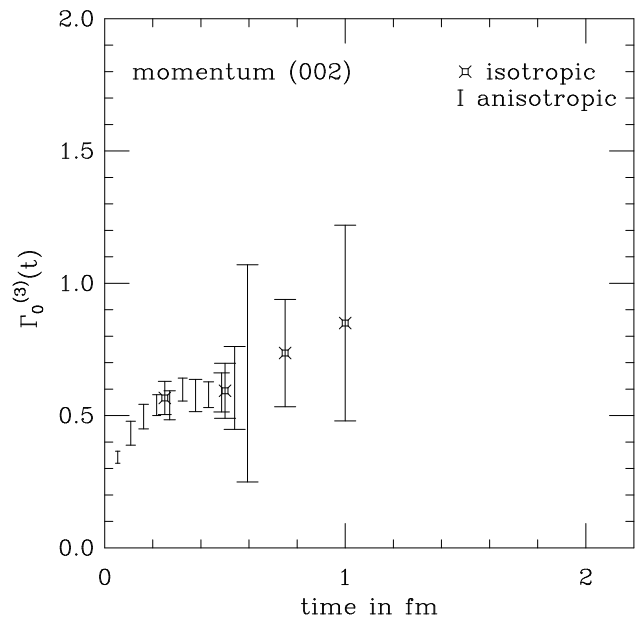
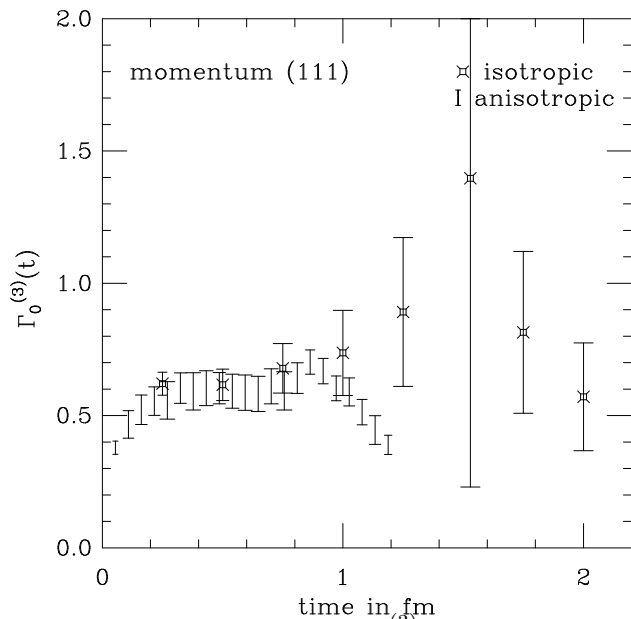


FIG. 22. $\Gamma_0^{(3)}(t)$ of eq.(34) for pion momentum (1,1,1) and (0,0,2).

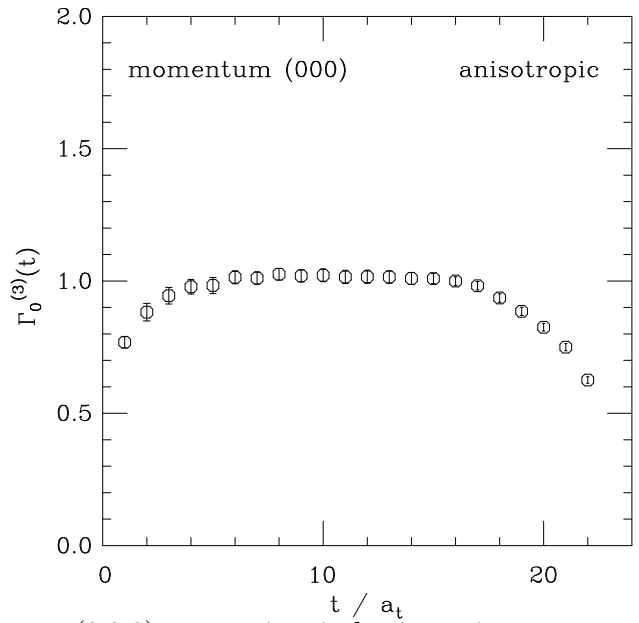
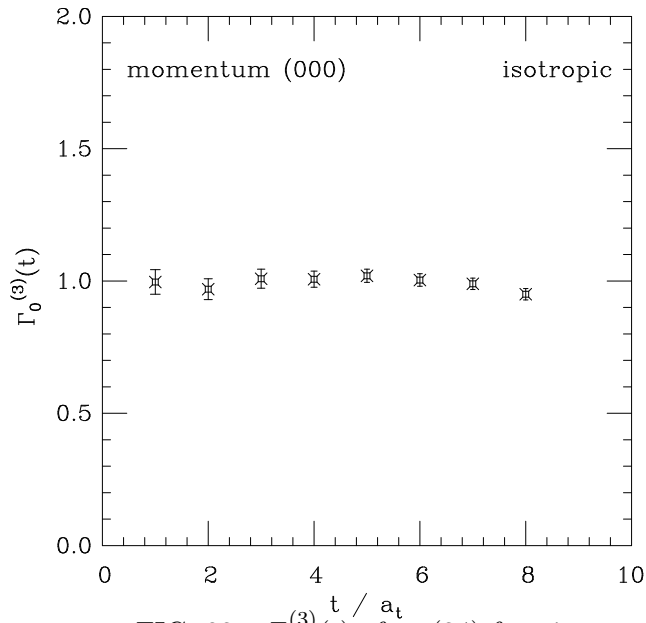


FIG. 23. $\Gamma_0^{(3)}(t)$ of eq.(34) for pion momentum (0,0,0) versus time in lattice units.

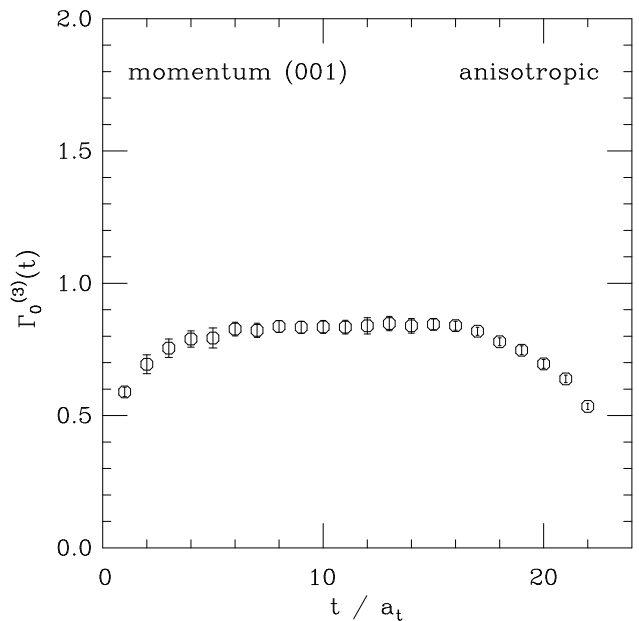
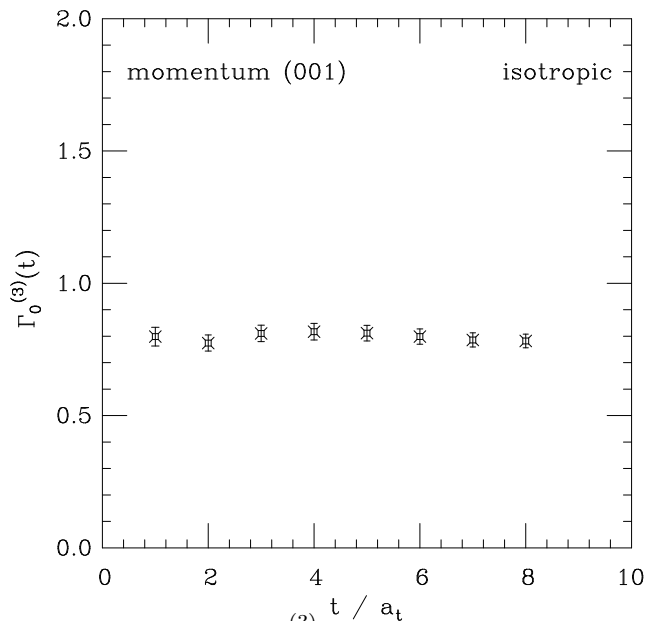


FIG. 24. $\Gamma_0^{(3)}(t)$ of eq.(34) for pion momentum (0,0,1) versus time in lattice units.

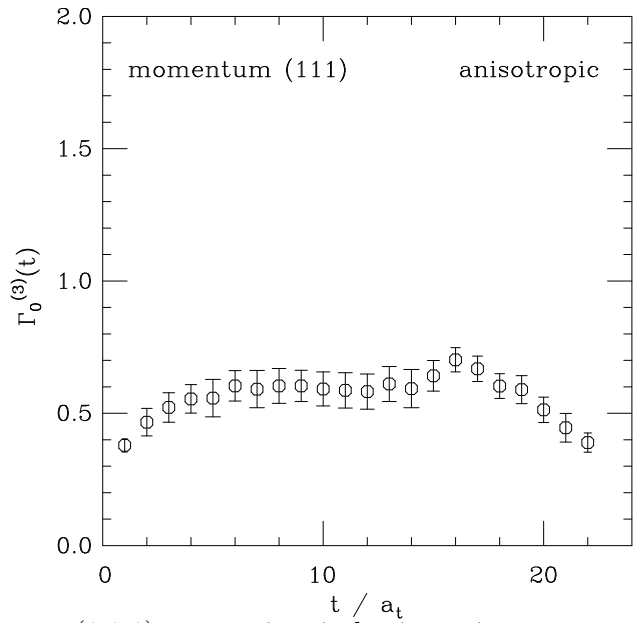
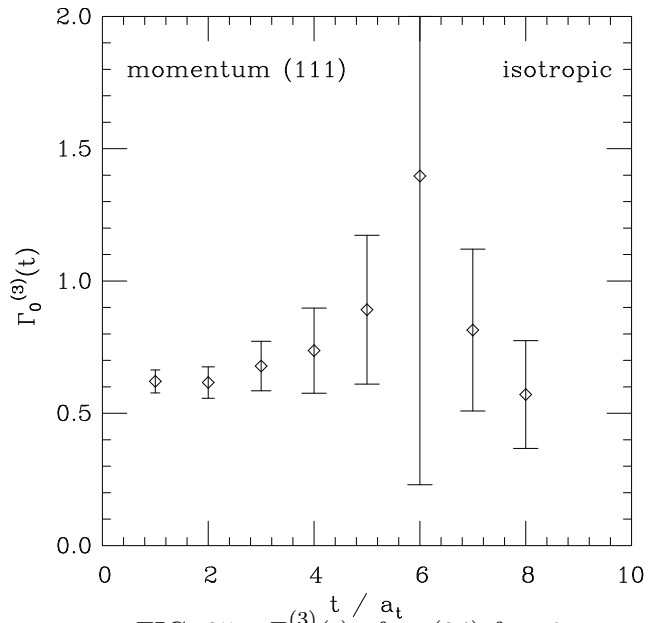


FIG. 25. $\Gamma_0^{(3)}(t)$ of eq.(34) for pion momentum (1,1,1) versus time in lattice units.

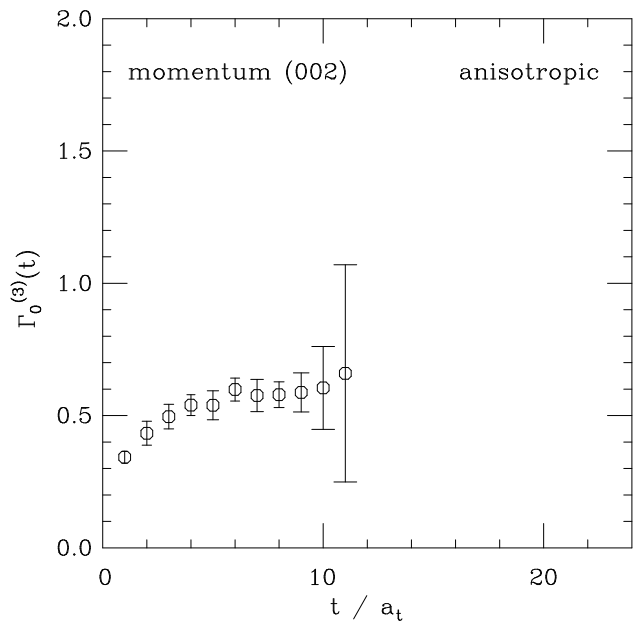
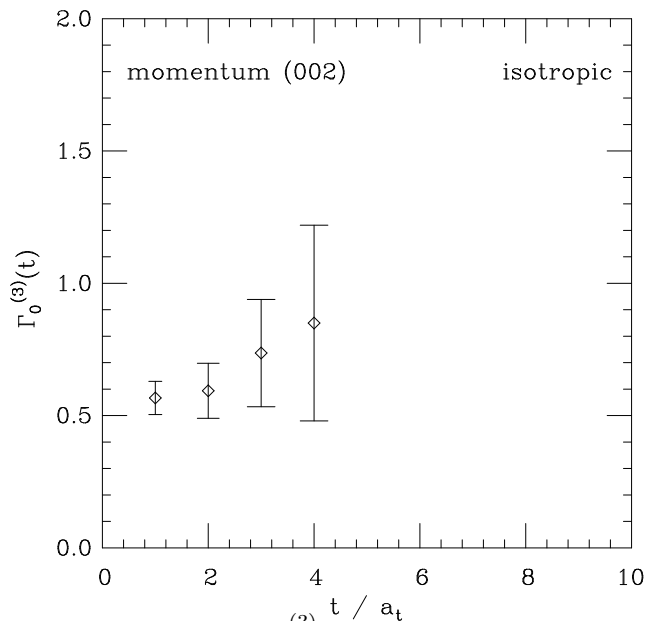


FIG. 26. $\Gamma_0^{(3)}(t)$ of eq.(34) for pion momentum (0,0,2) versus time in lattice units.

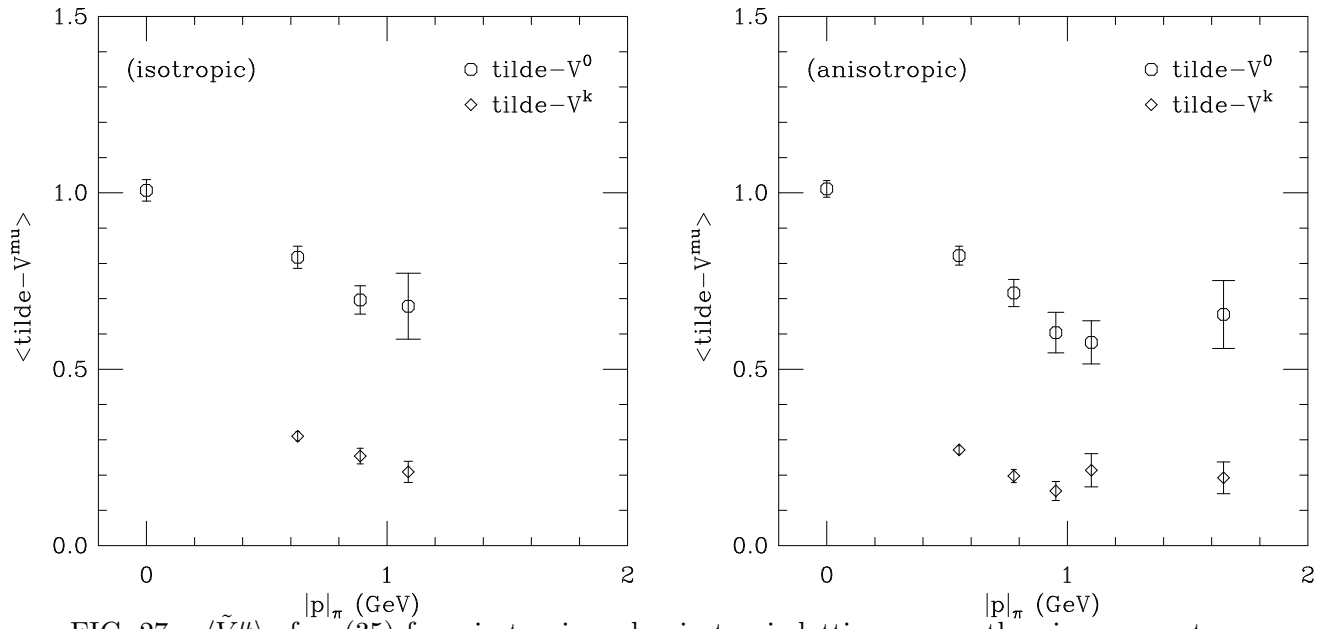


FIG. 27. $\langle \tilde{V}^\mu \rangle$ of eq.(35) from isotropic and anisotropic lattices versus the pion momentum.

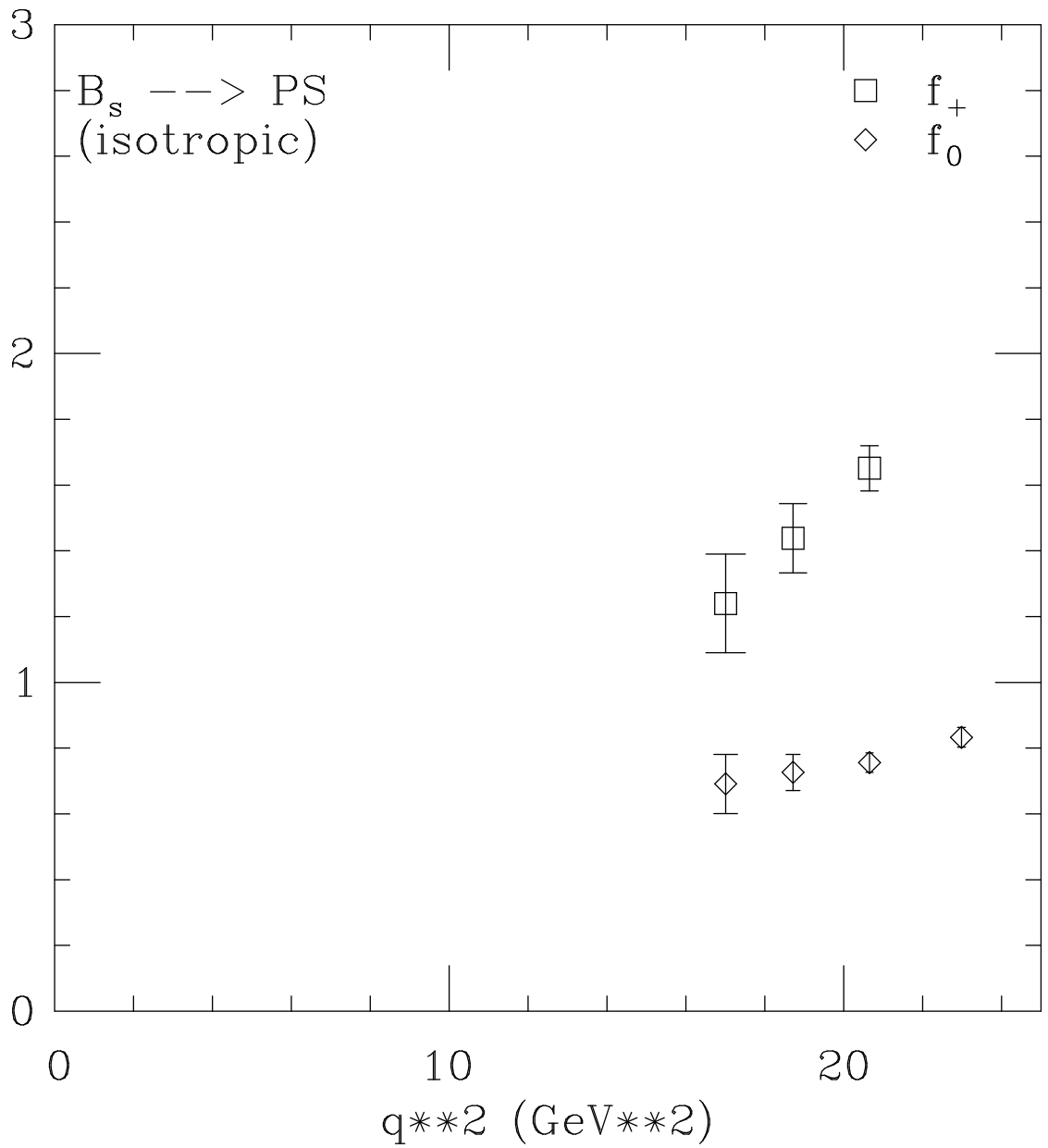


FIG. 28. The form factors $f_0(q^2)$ and $f_+(q^2)$ for B_s decays from isotropic lattices. See Table II for actual values of the decaying heavy meson and daughter meson masses.

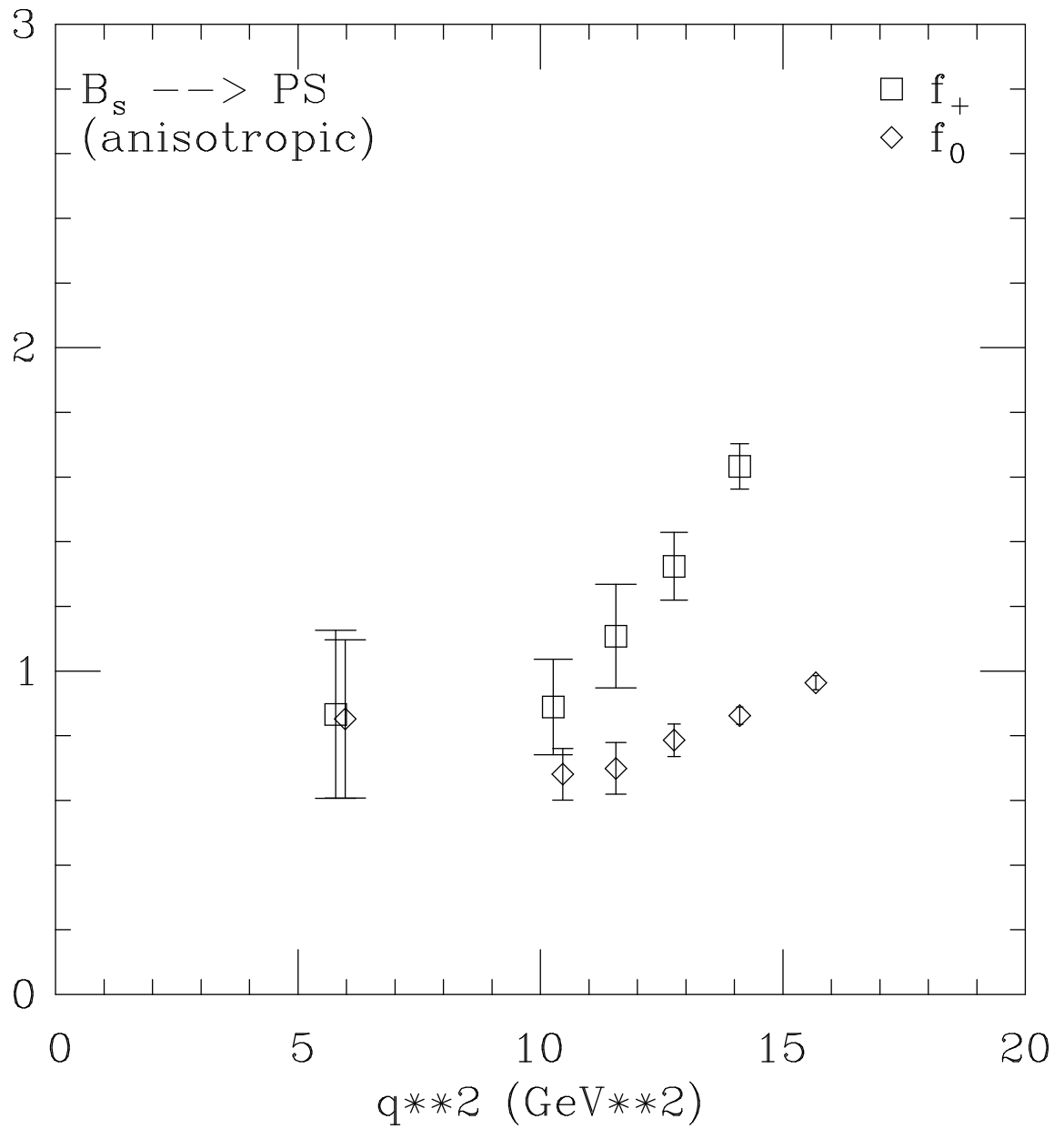


FIG. 29. The form factors $f_0(q^2)$ and $f_+(q^2)$ for B_s decays from anisotropic lattices. See Table II for actual values of the decaying heavy meson and daughter meson masses. Some points have been shifted horizontally for clarity.

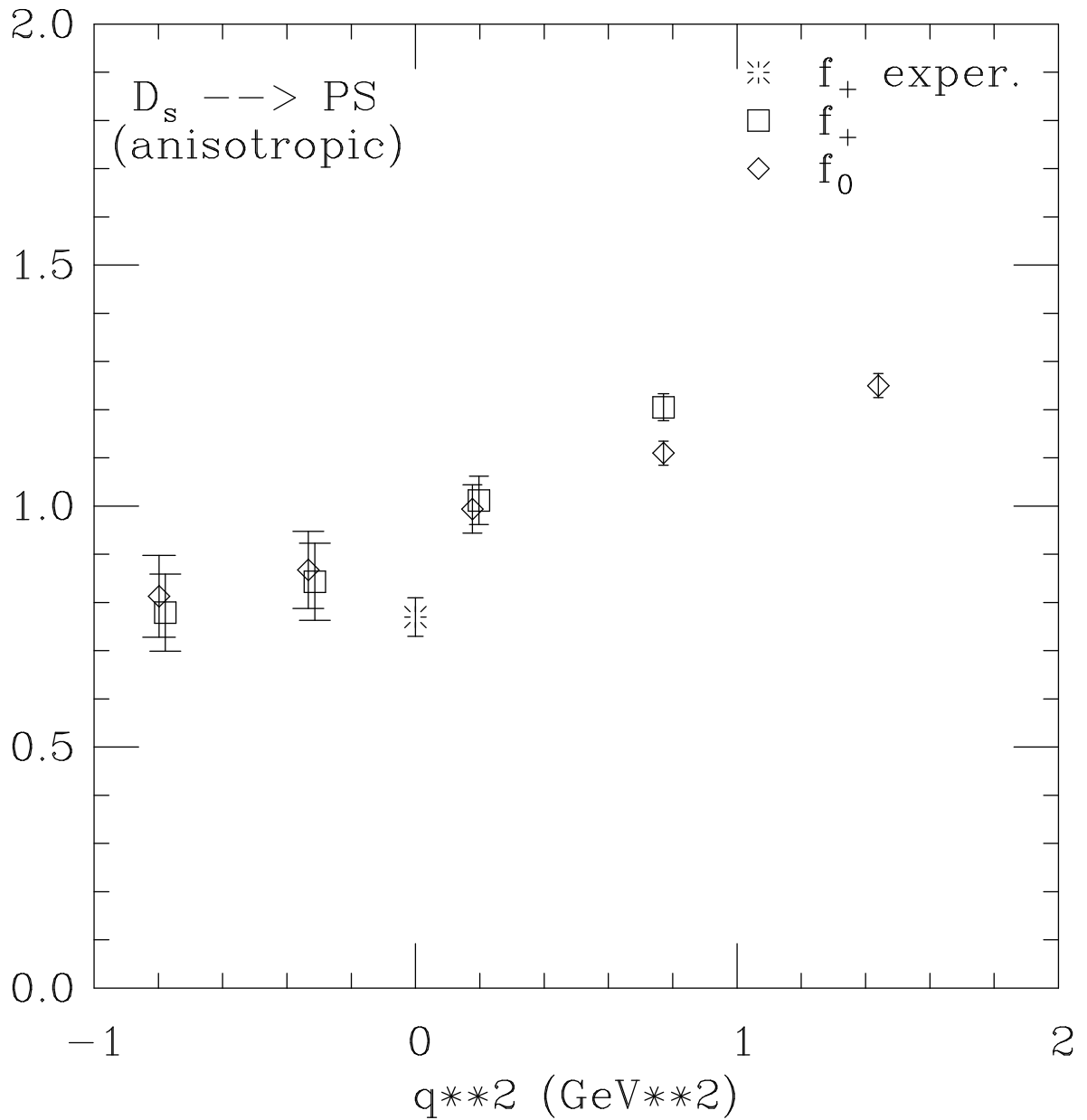


FIG. 30. The form factors $f_0(q^2)$ and $f_+(q^2)$ for D_s decays from anisotropic lattices. The “burst” shows an experimentally determined value of $f_+(q^2 = 0)$ for the decay $D^0 \rightarrow K^- l^+ \nu$ [34].